Photocatalysis of Ag-loaded $BaTiO_3$ and $CaTiO_3$ for degradation of Methylene blue dye under sunlight

Dissertation submitted in partial fulfillment of

the requirements for the award of degree of

Master of Science

in Chemistry

Submitted by: TIYA SARAS

Registration no.: 302302006

Under the guidance of
Dr. Bonamali Pal

Department of Chemistry and Biochemistry,

Thapar Institute of Engineering and Technology

Patiala-147004, Punjab, India

DECLARATION

I hereby declare that the dissertation, "**Photocatalysis of Ag-loaded $BaTiO_3$ and $CaTiO_3$ for degradation of Methylene blue dye under sunlight**", submitted to the Department of Chemistry and Biochemistry, Thapar Institute of Engineering and Technology, Patiala, in partial fulfillment of the requirements for the award of a Master of Science in Chemistry, is a record of my work that I conducted from January 2025 to July 2025 under the supervision of Dr. Bonamali Pal. The results contained in this dissertation have not been submitted in part or full to any other university or institute for the award of any other degree or diploma.

Date: 31-07-2025
Place: Patiala

(Tiya Saras)
Registration no. 302302006

CERTIFICATE

This is to certify that the dissertation entitled " **Photocatalysis of Ag-loaded $BaTiO_3$ and $CaTiO_3$ for degradation of Methylene blue dye under sunlight** " being submitted by Tiya Saras to the Department of Chemistry and Biochemistry, Thapar Institute of Engineering and Technology, Patiala, in partial fulfillment of the requirements for the award of degree of the Master of Science in Chemistry, is an authentic record of the work carried out by the candidate under our guidance and supervision. She has fulfilled the requirements for the submission of this dissertation, which, to our knowledge, has reached the requisite standard.

The results embodied in the dissertation have not been submitted in part or full to any other university or institute for the award of any other degree or diploma.

Date: 31/07/25

Place: Patiala

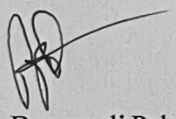

Dr. Bonamali Pal

(Professor)

ACKNOWLEDGEMENT

I would not have been able to complete this M.Sc. project without the assistance and advice I received from numerous individuals, and it has been a truly life-changing experience for me.

First and foremost, I would like to express my sincere gratitude to my supervisor Dr. Bonamali Pal for all of their support and inspiration. They have consistently offered technical materials, and we have had insightful discussions about the given topic, for which I am grateful. Without their inspiration and assistance, this accomplishment would not be complete.

I would like to express my gratitude to the Department of Chemistry and Biochemistry at Thapar Institute of Engineering and Technology for their invaluable help during this project. The kind help from the DST-FIST program for HRMS analysis (SR/FST/CS-11/2018/69). I would also like to express gratitude to DBT (BT/PR36172/NNT28/1811/2021), the CSIR project under the scheme (No.1(3082)/21/EMR-II), and the DST-PURSE program (SR/PURSE/2023/213) for research equipment.

I would like to express my gratitude to Dr. Davinder Kaur, my lab research scholar, for her patience, guidance, and sharing of her experience. I would also like to thank my labmates Kirti Bisht, Imran and my good friends Aniket, Sehaj, Manisha for helping and motivating me.Without them, this accomplishment would not have been possible.

Lastly, I would like to express my gratitude to my parents, in particular to my mother and father, for their unwavering and unselfish support in all aspects of my life-from moral to financial-during my dissertation and the years I spent studying.

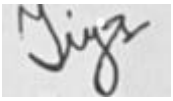

Date:30/07 /2025
Place: Patiala

Tiya Saras

ABSTRACT

Our research focuses on the fabrication of $BaTiO_3$ and $CaTiO_3$ by a hydrothermal method and improving its photocatalytic characteristics by loading it with Ag metal. This change allows the photocatalyst to efficiently absorb broad-spectrum solar light while also effectively separating charges, which are critical for photocatalysis. $CaTiO_3$ discovered to exhibit spherical shape, with Ag showing as smaller spheres. $BaTiO_3$ exhibit nanorod shape with Ag showing as smaller spheres. Both Ag loaded nanocomposites Ag-$BaTiO_3$ and Ag-$CaTiO_3$ photocatalysts effectively degraded Methylene blue dye under solar light exposure, degradaing 95% and 99.4% over 4h and 1h. Visible produced lower MB dye breakdown rates of 89% and 92% for $BaTiO_3$ and $CaTiO_3$ respectively, highlighting direct sunlight as our catalyst's most effective light source (99.4%). Reusability experiments showed the catalyst's high stability, with an 81.8% MB dye degradation efficiency after five cycles. Scavenger studies emphasized the crucial role of h+ active species in the photodecomposition process. Ag-$BaTiO_3$ and Ag-$CaTiO_3$, with its simple synthesis method and outstanding performance, is a promising alternative for eliminating persistent pollutants in textile wastewater systems.

Keywords: Ag-$BaTiO_3$ photocatalyst; Ag-$CaTiO_3$, Photocatalytic activity; Methylene blue ; Visible/Sunlight irradiatiosn,

TABLE OF CONTENTS

LIST OF ABBREVIATIONS

Mb: Methylene Blue

VB: Valence band

CB: Conduction band

DI: Distilled water

Wt%: Weight percentage

DRS: UV-Visible diffuse reflectance spectroscopy

FE-SEM: Field Emission scanning electron microscopy

HR-TEM: High resolution transmission Electron Microscopy

PL: Photo-luminescence

XRD: X-Ray diffraction

EDS: Energy-dispersive X-Ray spectroscopy

LIST OF SYMBOLS

K: rate constant

eV: electron volt

a.u: arbitrary unit

%: percentage

rpm: resolution per minute

mg: milligram

1. INTRODUCTION AND LITERATURE REVIEW

1.1 Introduction

At present, approximately 100,000 different types of dyes are produced globally with an annual production rate of 700,000 tons., in which textile industry is a significant consumer of dyes, with around 36,000 tons of dye consumed annually [1]. About 12% of dyes are excluded as waste during the dyeing process and nearly 20% of these dyes end up in the environment, contributing to water pollution and harming aquatic ecosystems[2], [3]. Azo dyes are the common synthetic organic dyes used in the textile industry, hence being the most common industrial pollutant. They are characterized by the presence of one or more azo group (–N=N–) bound to aromatic rings[4][5]. These are produced in large amounts, and when they enter the environment during the production and manufacturing process, make water toxic, carcinogenic, and mutagenic. The removal of dyes and other pollutants from the aqueous environment has become a challenging task in recent years. To protect the environment, various methods have been used, such as ozonation, membrane filtration ,bioadsorption, ion exchange removal, adsorption[6], photocatalytic degradation ,catalytic reduction [7], biological/aerobic treatment and coagulation. Compared with conventional technologies, advanced oxidation processes (AOPs) have also been developed beneficial for the degradation of dyes .[8] AOPs include ozonation[9], photocatalysis [14], the Fenton/photo-Fenton method[10] ,electrochemical oxidation and ionizing radiation. Recent studies [11], [12] shows that for the removal of dye from waste water, photocatalytic method is preferred as it completely mineralize the target pollutants.

Heterogenous catalyst is getting more and attention as it can utilize sunlight as a source of energy[13] and also due to increasing pollution.[14].In heterogeneous catalysis on the absorption of light, electrons are transferred from the valence band to the conduction band leaving holes(h+) behind. In the VB, h+ will react with H_2O/OH^- to produce a hydroxyl radical (•OH) via an oxidation reaction. In addition, The electrons (e-) in the conduction band (CB) react with oxygen molecules (O_2) to generate superoxide anion radicals (O_2•-) through a reduction reaction. The superoxide anion radicals can further react with hydrogen ions (H+) to form hydroperoxyl radicals (HO2•), which can then react with other superoxide anion radicals to produce hydrogen peroxide (H_2O_2). H_2O_2 increases the rate of formation of hydroxyl radical as H_2O_2 is reduced at the conduction band and self-decomposition by irradiation (So et al. 2002;

Lee et al. 2003). The highly reactive ROS such as hydroxyl radicals (•OH) and superoxide anion radicals (O2•-) generated through this process can interact with hazardous organic pollutants in water or wastewater, leading to their degradation. $H_2O_2 + O_2^{\cdot-} \rightarrow {}^{\cdot}OH + OH^- + O_2H_2O_2 + hv \rightarrow 2{}^{\cdot}OH$. These ROS are the majorly responsible for the degradation of persistent organic pollutants in wastewater, The reactive radicals can break down the organic pollutants into smaller fragments, ultimately converting them into carbon dioxide (CO_2) and water (H_2O).[15].

Many photocatalysts like TiO_2, CuO, ZnO, Fe_2O_3, $MTiO_3$ (*M* = Sr, Ca, Ba), CdS, ZnSe etc. are used to degrade dyes[18]. Titanate perovskites are mostly used due to their resemblance to TiO_2. (30) Titanates with general formula $ATiO_3$ appear to be promising photocatalysts due to their polyvalent properties for piezoelectric, ferroelectric, optoelectronics, and photocatalytic applications. (13) $CaTiO_3$ has a perovskite structure having the general formula ABO_3. It has a high dielectric constant, ferroelectricity, chemical stability, low dielectric loss, economically friendly, and it has a significantly higher negative conduction band edge potential, making it for effective catalyst[19][20]. It is cited in the literature as a promising photocatalyst alternative to TiO2 due to its wider band gap energy (~3.6 eV) and unique properties that favor its use in heterogeneous photocatalysis, whereas the band gap of TiO_2 is around 3.2 eV according to the literature [21]. $BaTiO_3$ is one of the emerged promising semiconductor photocatalyst for removing hazardous organic pollution from wastewater due to its high dielectric/ferroelectric/piezoelectric properties, low cost, low toxicity, environmental friendly, perovskite structure, availability in a wide variety in term of sizes and morphologies, multiple crystal phases, flexibility, good stability and appropriate value of band gap[22]

For the synthesis of $CaTiO_3$ and $BaTiO_3$ various methods have been developed. High-purity $BaTiO_3$ powder has been synthesized using various chemical methods, including barium tetanyl oxalate, hydrolysis of barium titanium alkoxide, co-precipitation, one-step sol-gel, molten salt, and hydrothermal processes. The hydrothermal synthesis method involves reactions in a strong alkaline solution to produce high-purity, homogeneous, and ultrafine BaTiO3 powder at relatively low temperatures (60-180 °C). In the current investigation $CaTiO_3$ and $BaTiO_3$ were synthesized through hydrothermal method[23], [24] .

Although $BaTiO_3$ and $CaTiO_3$ are highly photoactive materials, due to their wide band gap and low quantum efficiency, their overall photocatalytic efficiency has been lowered. It can be understood primarily by two reasons: fast recombination of electron-hole pairs and the limited optical response only to UV-light (Due to a large band gap)[25][26]. High E_g value will require

more energy to be absorbed to deliver charge carrier separation. In addition, the electrons and holes could recombine with each other without participating in photocatalytic reactions. If the recombination rate is very fast, it will result in a lower number of photo- generated ROS that will be available on surface reaction sites for the photo-degradation process. Hence, it will hinder the overall photocatalytic quantum efficiency (Koe et al., 2020). To increase their photocatalytic activity, recombination should be prevented, and the range of optical response should be broadened. Various methods have been developed to boost the efficiency of photocatalyst by doping to reduce the band gap of Photocatalyst and increasing the charge carrier separation by composing photocatalysts with layered materials or other compounds to form heterostructures.

The synthesized nanocomposites $BaTiO_3$ and $CaTiO_3$ were evaluated for their effectiveness in degrading Methylene Blue (MB) dye. The photocatalytic activity of $BaTiO_3$ and $CaTiO_3$ nanocomposites was assessed through a series of tests, The metal-loaded nanocomposites were refined to optimize their photocatalytic activity.including reaction kinetic analysis(to understand the degradation mechanism.), recyclability assessment(to determine their stability and potential for repeated use.), and active species detection tests(understand the degradation mechanism).

Photocatalytic efficiency of titanates can be effectively increased by various elements like Ag, Ce, Cr, Fe, Mo, Mn, Ni, Rh, V, W and Zn which can shift the bandgap to the visible region for better efficient[22]. Among all noble metal, Ag has been used widely as a dopant.[27]Several authors have reported that introduction of Ag+ ions in semiconductor can generate the intrinsic defects that can modify the photocatalytic properties of semiconductor[28][29] [9]. Using Ag as a doping agent, leads to a red-shift thus increasing photocatalytic efficiency of photocatalyst in the visible-light region[30]. Since Ag metal is a good conductor, it can act as a sink for free electrons and increases the separation rates of photo-induced electron-hole pairs. Noble metal nanoparticles (NPs), like gold or silver, have a special property that allows them to absorb visible light and create a phenomenon called localized surface plasmon resonance (LSPR).[31], [32]This LSPR effect generates a strong electromagnetic field around the nanoparticles. The

field can help create and separate pairs of electrons (e-) and holes (h+) in nearby semiconductor materials[33]

Methylene blue (MB) is one of the materials most heavily used in the dye industry. It's often used to colour various materials like silk, wool, cotton, and paper[34]. MB is toxic, carcinogenic, and non-biodegradable dye thus causing serious threat to human health and have adverse effects on the environment[35]. Treatment of wastewater containing MB dye before discharging into the environment is of great importance due to its harmful impacts on water quality and perception. In this paper methylene blue has been taken.

The report examines the photocatalytic performance of Ag-doped $CaTiO_3$ and $BaTiO_3$ (containing 2 wt% Ag). Hydrothermal synthesis was used for the production of photocatalysts, and subsequently, Ag was doped using the photo-deposition method. The prepared samples were thoroughly characterized by X-ray diffraction (XRD), diffuse reflectance spectroscopy (DRS), photoluminescence (PL), Field Emission scanning electron microscopy (FE-SEM), high-resolution mass spectroscopy (HRMS), and energy dispersive spectroscopy (EDS). The photocatalytic performance of the photocatalysts was examined by removing methylene blue dye under sunlight. The doped samples showed more photocatalytic activity in the degradation of MB dye in comparison to the undoped samples.

1.1 Objectives

1) Preparation and characterization of $BaTiO_3$, $CaTiO_3$ and the photo deposition of noble metal Ag on it.

2) To study the various physiochemical properties of Ag-modified $BaTiO_3$ and $CaTiO_3$ nanocomposites.

3) To study the photocatalytic degradation of methylene blue dye by Ag-$BaTiO_3$ and Ag-$CaTiO_3$ nanocomposites under visible illumination and solar light.

2. EXPERIMENTAL SECTION

2.1 Apparatus

Beakers, measuring cylinder, Weighing balance, Stirrer, Muffle furnace, Spatula, Magnetic beads, Centrifuge tubes, Mortar and pestle, Hot air oven

2.2 Chemical and Reagents

Calcium Nitrate Hexahydrate ($CaNO3.6H_2O$), Barium Sulphate ($BaSO_4$), Titanium Dioxide ($P25\text{-}TiO_2$), Sodium Hydroxide Pellets (NaOH), Isopropyl Alcohol (IPA), Silver nitrate ($AgNO_3$), Methylene Blue, Ethanol

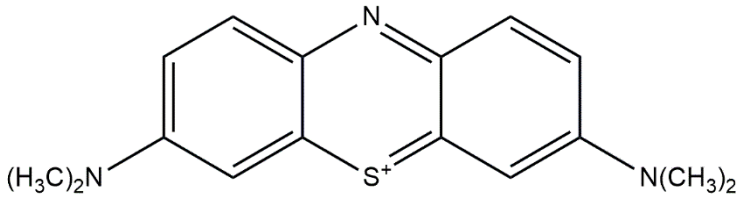

Fig.1: Structure of Methylene Blue.

2.3 Synthesis of $CaTiO_3$

Scheme 1: Calcium Titanate was synthesized by Hydrothermal Method. 0.8g of Calcium Nitrate ($CaNO_3.6H_2O$), 0.2g TiO_2, 40g NaOH mixed in 100mL D.I water. The obtained mixture was stirred for 1h. Then the mixture was loaded to a Teflon lined autoclave (100mL) and treated hydrothermally at 200°C for 12h. After the mixture was cooled, the precipitates were centrifuged and washed multiple times with distilled water and absolute ethanol, then dried at 60^oC overnight.

2.4 Synthesis of Ag-$CaTiO_3$ nanocomposite

Scheme 3: Photodeposition method was used for the fabrication of nanocomposite. A mixture of Isopropyl alcohol - distilled water (1:1) along with 1852ul of 0.01mM $AgNO_3$ solution (2% Ag- loaded $CaTiO_3$) was prepared in a test tube. The prepared $CaTiO_3$ powder (100mg) was added in the test tube and test tube was tightly closed by a rubber septum. Then the test tube was purged with argon gas for 15min. The test tube was constantly stirred for 2h under illumination of UV radiations in photochemical reactor. The test tube was constantly stirred for 2h under illumination of UV radiations (125W, $10.4mW/cm^2$) in photochemical reactor. The precipitates were then centrifuged and washed multiple times with distilled water and absolute ethanol, then dried at 60^oC.

2.5 Synthesis of $BaTiO_3$

Scheme 2: For the synthesis of $BaTiO_3$ Hydrothermal Method was used. Firstly, solution A was prepared by dissolving 3mmol (733mg) of $BaSO_4$ in 20mL of distilled water. Then solution B was prepared by dissolving 3mmol (239mg) of TiO_2 in 20mL of distilled water. Similarly, solution was prepared by dissolving 0.2mol(8mg) of NaOH in 40mL of Distilled water. Then solution A and B were stirred for 1h. Solution B was mixed in solution A, followed by solution C drop wise. The obtained mixture was stirred for 1h. Then the mixture was loaded to a Teflon lined autoclave (100mL) and treated hydrothermally at 180°c for 12h. After the mixture was cooled, the precipitates were centrifuged and washed multiple times with distilled water and absolute ethanol, then dried at 60°C. Obtained white powder was calcinated in the muffle furnace at 700°C for 3h.

2.6 Synthesis of Ag-$BaTiO_3$ nanocomposite

Scheme 3: The photodeposition method was used for the fabrication of the nanocomposite. A mixture of Isopropyl alcohol - distilled water (1:1) along with 1852ul of 0.01mM $AgNO_3$ solution (2% Ag-loaded $BaTiO_3$), was prepared in a test tube. The prepared $BaTiO_3$ powder (100mg) was added to the test tube and test tube was tightly closed by a rubber septum. Then the test tube was purged with argon gas for 15 minutes. The test tube was constantly stirred for 2h under illumination of UV radiation in a photochemical reactor. The test tube was constantly stirred for 2h under illumination of UV radiation (125W, 10.4mW/cm^2) in a photochemical reactor. The precipitates were then centrifuged and washed multiple times with distilled water and absolute ethanol, then dried at 60°C.

2.7 Characterization techniques

The produced samples were subjected to crystallographic examinations using an X-ray powder diffraction Analytical-Xpert-PRO machine with a radiation source (1.54 Å) that operated at 45 kV and a diffraction angle (2θ) that ranged from 5° to 90° at a 5°/min scan rate. The photoluminescence (PL) emission spectrum was measured using a spectrofluorometer (Perkin-Elmer LS55), to investigate the separation of photogenerated electron-hole pairs. Both high-resolution transmission electron microscopy (HRTEM TALOS F200S G2 model running at 200 kV voltage) and scanning electron microscopy (SEM; JEOL JSM-7600F operated at 30 kV) were used to analyze the materials' size and

shape. The elemental composition ratio was analyzed using energy-dispersive spectroscopy (SEM-EDS, JEOL JSM-7600 F) at 30 kV. The optical absorption properties of powder solid samples were obtained using an Avante's DRS instrument and a UV-vis spectrophotometer (JASCO, V-750), over a spectral range of 200-800 nm, with $BaSO_4$ as a reference standard

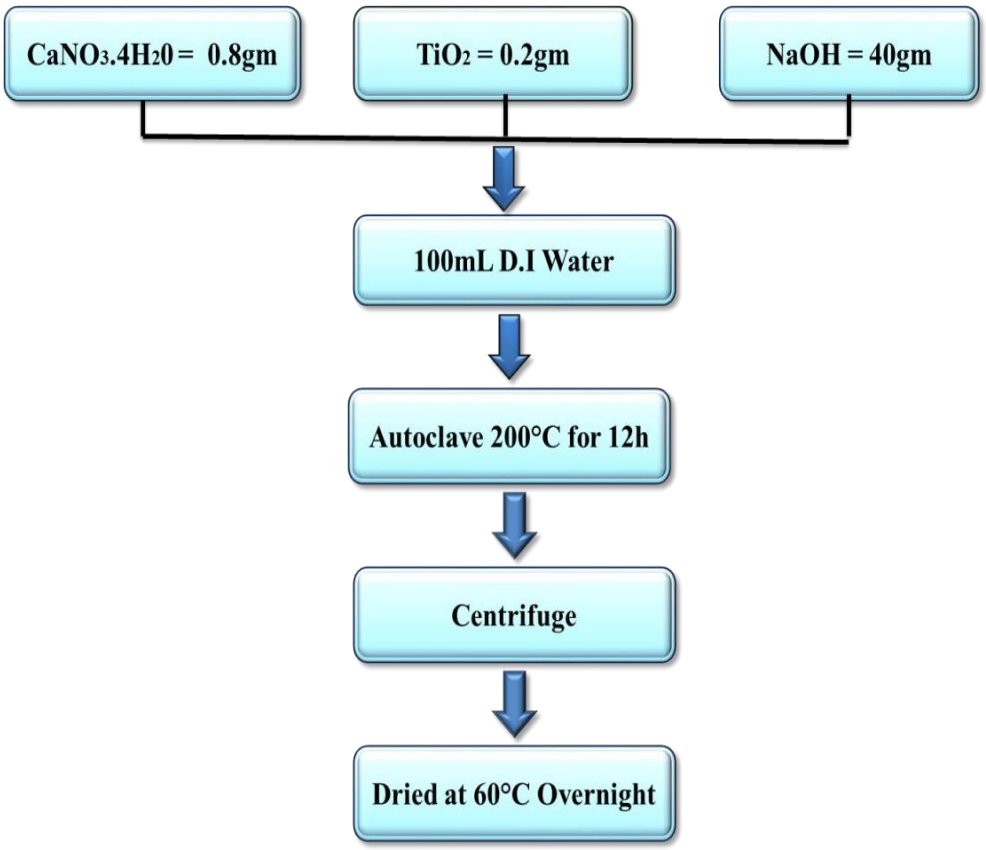

Scheme 1: Flow chart for synthesis of $CaTiO_3$.

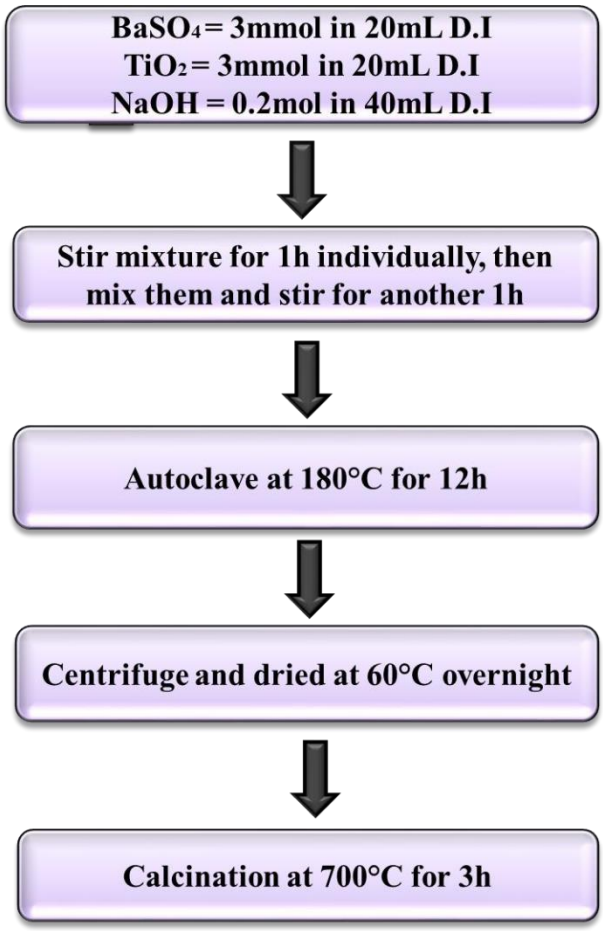

Scheme 2: Flow chart for synthesis of $BaTiO_3$

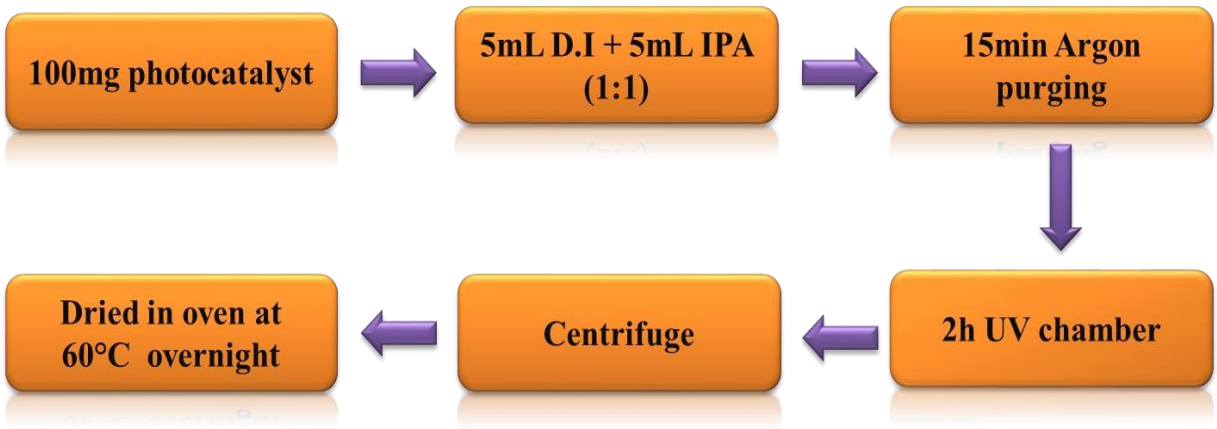

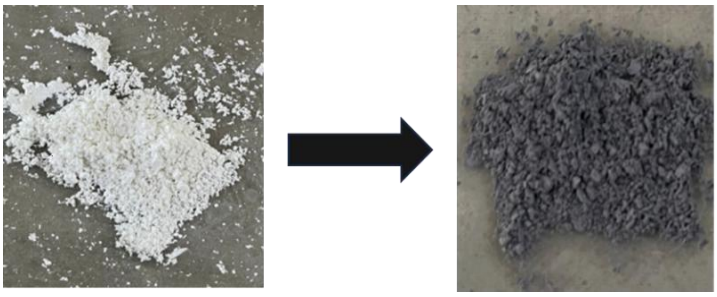

Scheme 3: Experimental procedure for photo-deposition of Ag nanoparticles onto photocatalyst..

2.8 Photocatalytic activity tests

The photocatalytic activity of $BaTiO_3$, $CaTiO_3$ and their composites (Ag-$BaTiO_3$ and Ag-$CaTiO_3$) was examined by the degradation of toxic dye Methylene Blue. For the degradation of MB Dye, 5mg of photocatalyst was taken in 10mL of 5ppm MB solution. Before irradiation, the suspensions were agitated in the absence of light for 2h to establish an Equilibrium of adsorption and desorption processes between the dye molecules and the catalyst's surface. The test tubes were illuminated with visible light for different time intervals. At a particular time interval, test tubes were centrifuged to remove the catalyst particles completely. After removing the catalyst, roughly 5–6 mL of the solution was taken out and absorbance of the solution was checked using a UV-Visible spectrophotometer. The photocatalysis studies occurred at the Thapar University in Patiala, India, in a subtropical region. The study spanned from April 1 to May 10, 2025. The solution was exposed to visible illumination from a 45 W CFL lamp (Philips) at a brightness of approximately 100 W/m^2 . UV light was applied to the solution using a 100 W Hg lamp at 365 nm with a flux density of 64–66 W/m^2. Each experiment was performed three times, and graphical representations were created with error margins representing a 3% data source error. The absorbance spectrum of Methylene Blue dye was measured at frequent intervals, specifically at λ_{max} = 665 nm.

The photocatalytic efficiency was measured by the following equation:

Degradation efficiency $= [(C_0 - C_t)/C0]100\%$

Where C_o and C_t are the initial conc. of dye and the conc. Of dye after irradiation of light for time.

The reaction rate constant, reflecting changes in the dye concentration during the reaction, was estimated according to the Beer-Lambert law:

$$t = -\ln(i/C0)$$

where k is the constant reaction rate, and t is the reaction time.

3: RESULTS AND DISCUSSION

3.1 Surface structural studies:

XRD (X-ray diffraction): The phase purity and crystallographic structures of the synthesized samples pure $BaTiO_3$, $CaTiO_3$, Ag-$BaTiO_3$ and Ag-$CaTiO_3$ composites, were examined from the XRD patterns, and the results are depicted in Fig. 2. XRD pattern of $CaTiO_3$ shows a prominent peak at 2θ = 23.3◦, 27.4◦, 33.1◦, 37.2◦, 39.0◦,40.8◦, 47.5◦, 53.9◦, 59.1, 62.4◦, 69.5◦, and 79.2◦ could be perfectly indexed to the respective (1 10), (1 1 1), (121), (102), (031), (220), (202), (311), (123), (231), (242), and (161) planes of the orthorhombic CaTiO3 (JCPDS card no: 42–0423). The XRD pattern of Ag-$CaTiO_3$ has two low-intensity peaks at 2θ values of 38.2 and 44.1, which relate to the (111) and (200) planes of metallic Ag, respectively(99). These peaks are denoted with star in the graph. However, a small decrease in the intensities of these peaks was observed on metal loading, which might be attributed to the suppression of the electron scattering of bare CTO upon loading of these heavy metals to its surface.[25] The diffraction peaks located at 2θ values 22.46◦ , 31.59◦ , 39.0◦ , 45.60◦ , 50.92◦ , 56.43◦ , 65.76◦ , 70.82◦ , 75.26◦ , 79.41◦ , 83.72◦ matches well with the (100), (101), (111), (200), (210), (211), (220), (212), (310), (311) and (322) lattice planes for $BaTiO_3$. (JCPDS No. 75-2122) respectively[36]. The XRD pattern of Ag-$BaTiO_3$ has two low-intensity peaks at 2θ values of 38.2 and 44.1, which relate to the (111) and (200) planes of metallic Ag, respectively (PDF-04-0783)[37]. The fact that the silver nanoparticles are well-loaded or disseminated on the surface instead of being embedded into the $CaTiO_3$ and $BaTiO_3$ lattice is further supported by the fact that the $CaTiO_3$ and $BaTiO_3$ peak location did not alter. However, there is a small decrease in the intensities of peaks on metal loading, which might be attributed to the suppression of the electron scattering upon loading of metal to its surface.

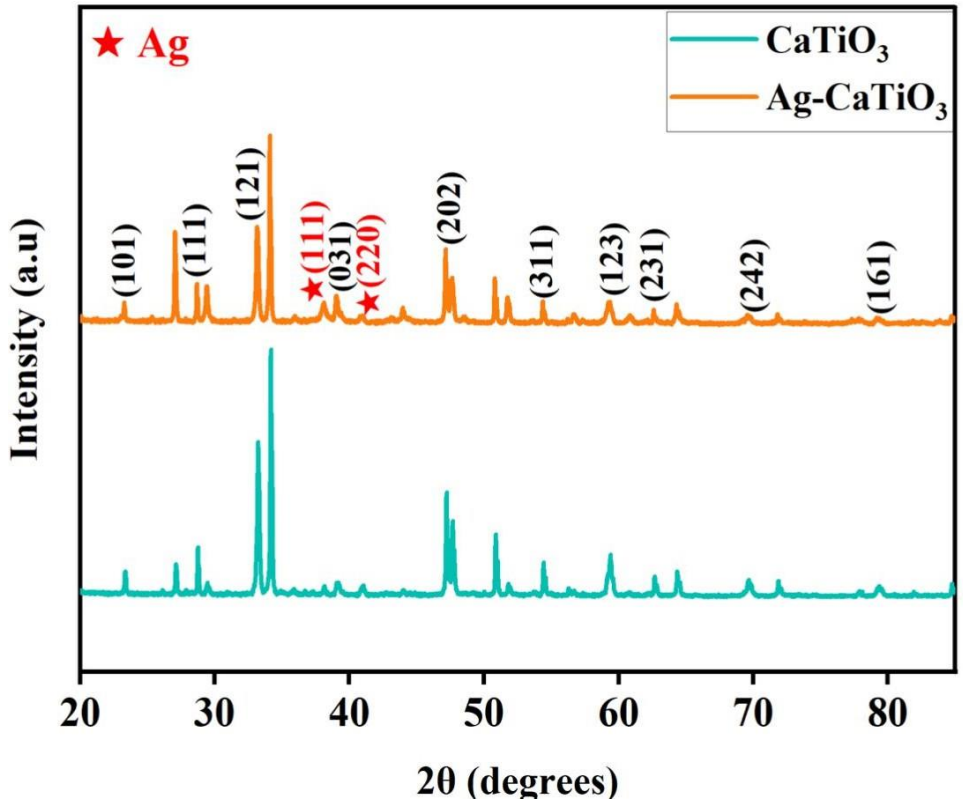

Fig. 2: XRD graph of $CaTiO_3$ and Ag-$CaTiO_3$.

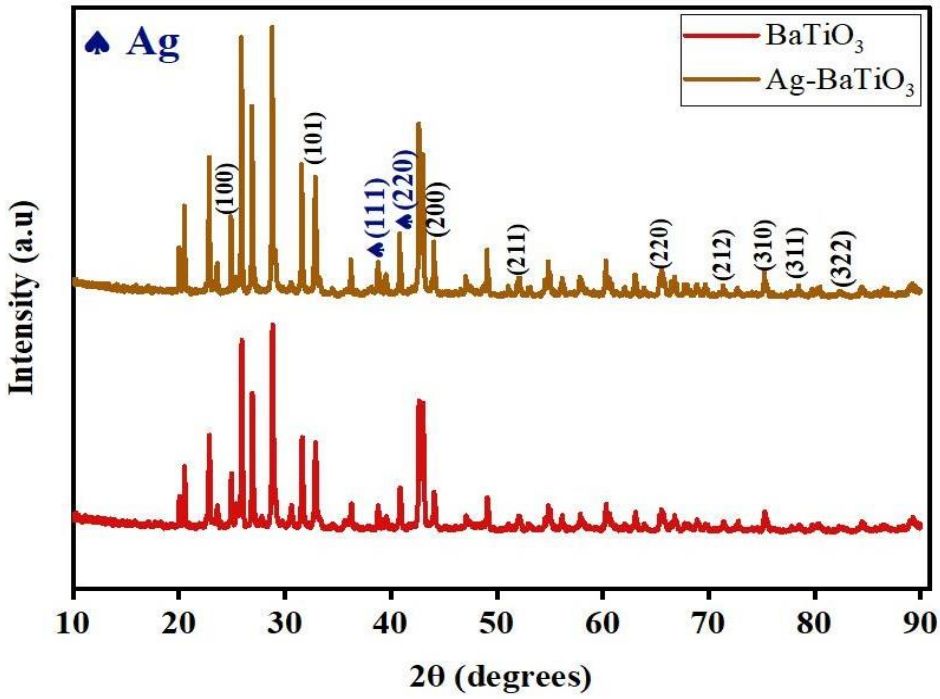

Fig.3 XRD graph of $BaTiO_3$ and Ag-$BaTiO_3$.

3.2 Morphological study:

The surface morphology of the catalysts was identified by FE-SEM and HR-TEM analyses. Fig. 4(a)-(d) shows FE-SEM images of $CaTiO_3$, and Fig.6(a)-(d) shows FE-SEM images of Ag-$CaTiO_3$. Mostly cuboidal aggregates or clusters were obtained for the samples. Fig. 8(a)-(b) shows FE-SEM images of Bare $BaTiO_3$ and Fig. 8(c)-(d) shows FE-SEM images of Ag-$BaTiO_3$. FE-SEM was unable to distinguish between pure and silver deposits due to low wt% deposition of Ag. However, the elemental composition data shows the presence of Ag on the $BaTiO_3$ and $CaTiO_3$ surfaces. EDS analysis was utilized to determine the amount of elements found in the composite materials. materials. Separate EDS spectra of prepared samples are shown as Fig.5 $CaTiO_3$, Fig.7 Ag-$CaTiO_3$ and Fig9(a)-(b) $BaTiO_3$ and Ag-$BaTiO_3$. The amount of Ag loaded was 2wt%, whereas the observed value was 0.44% and 0.03%. The possible reason of reduced Ag concentration could be attributed to selected area selection for EDX, mass loss during photo deposition, or washing.

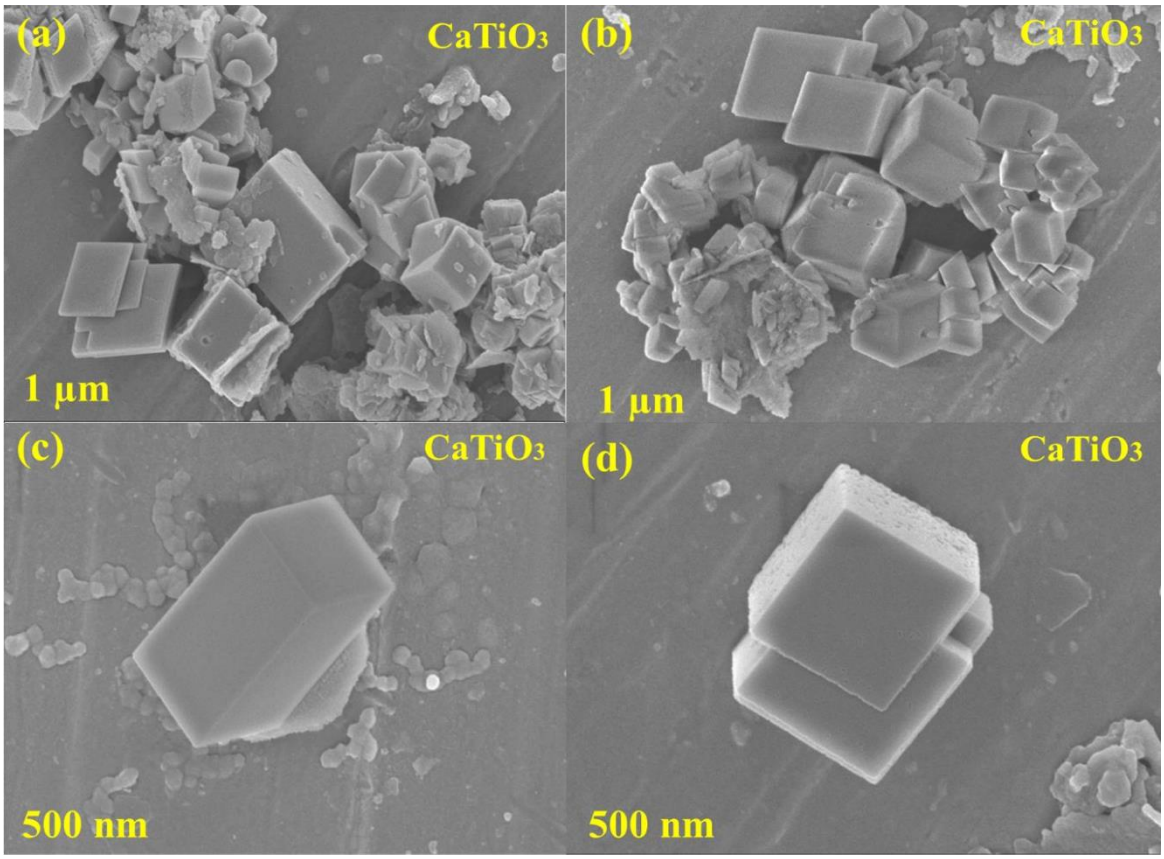

Fig.4: FE-SEM images of $CaTiO_3$.

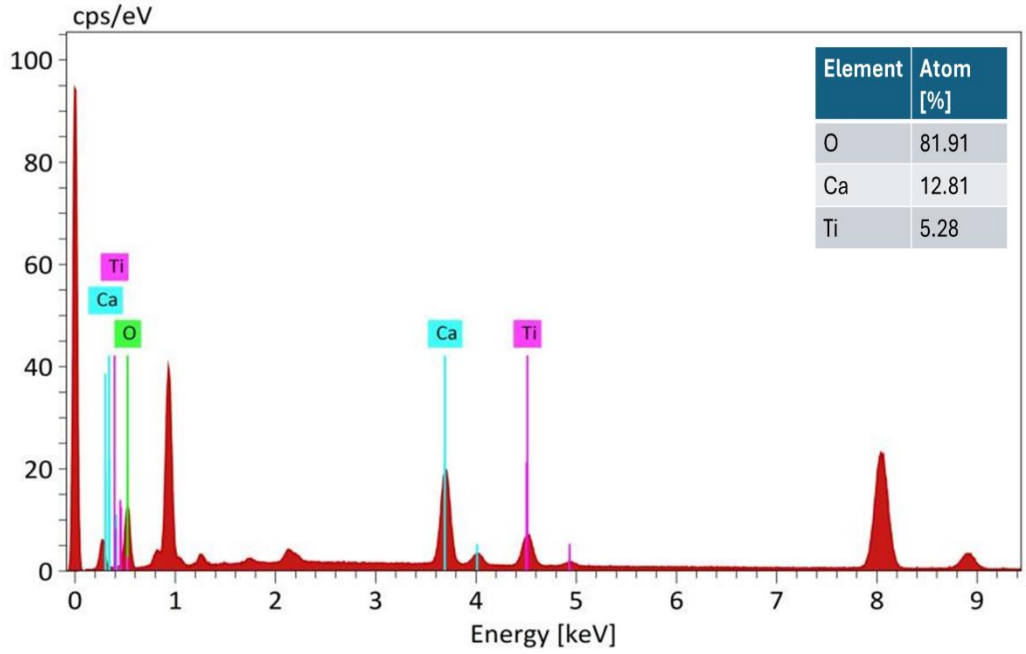

Fig.5: EDS analysis of $CaTiO_3$.

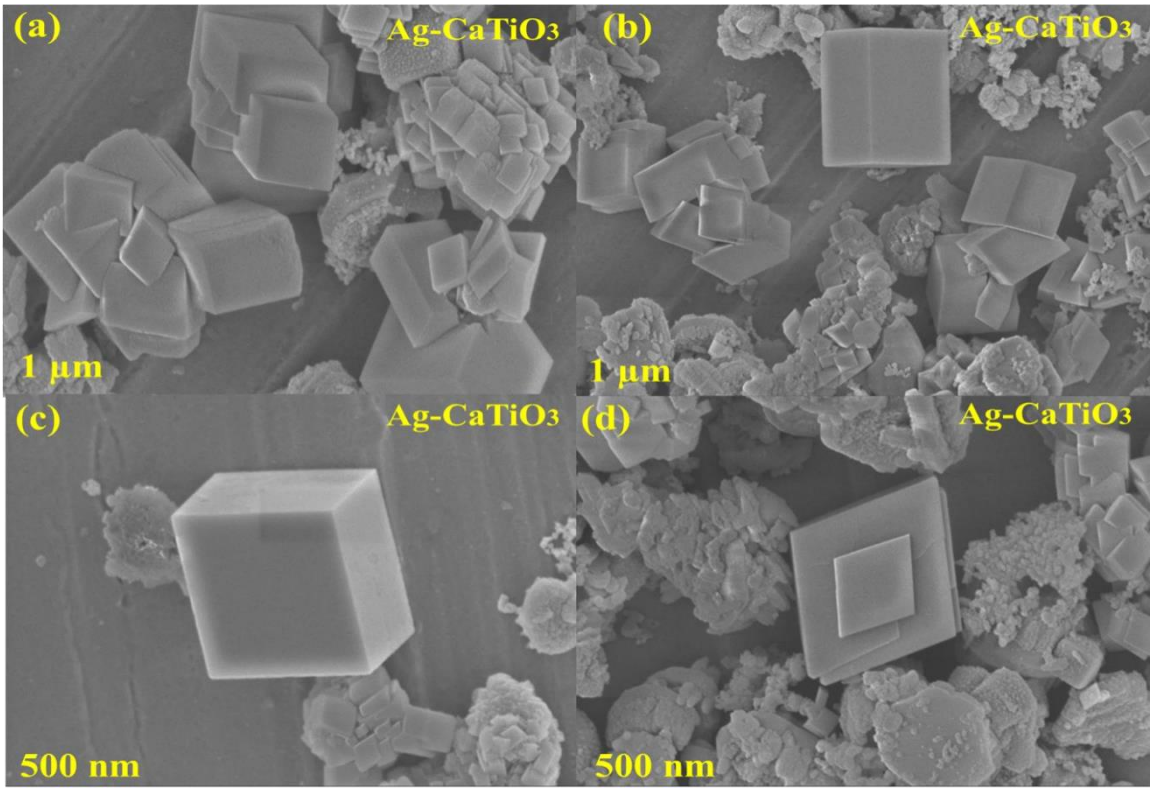

Fig.:6 FE-SEM images of Ag-$CaTiO_3$.

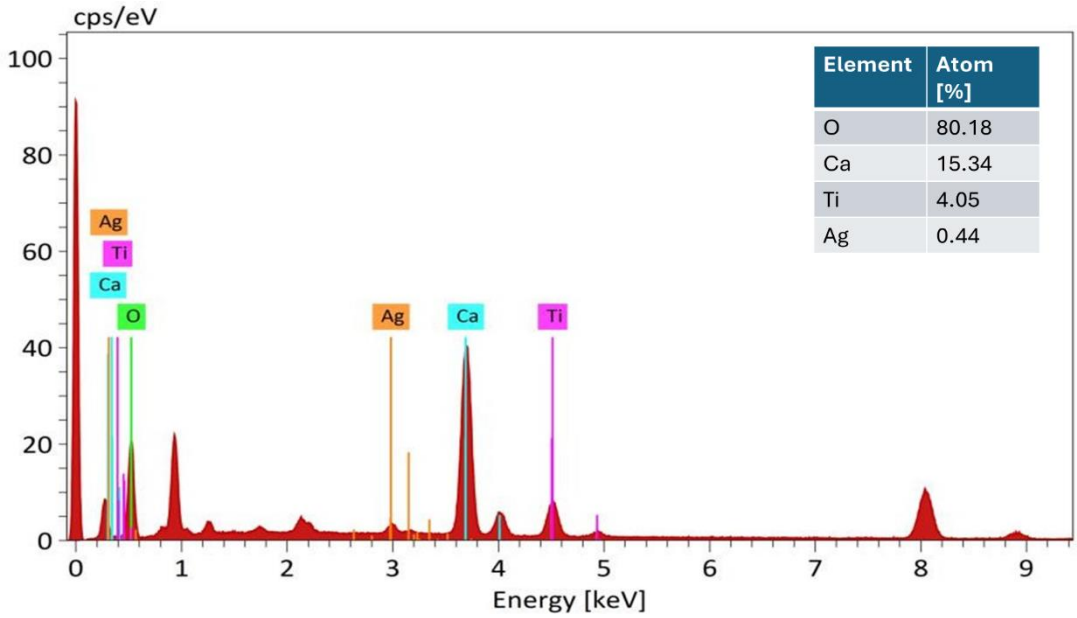

Fig.7: EDS analysis of 2wt% Ag loaded $CaTiO_3$.

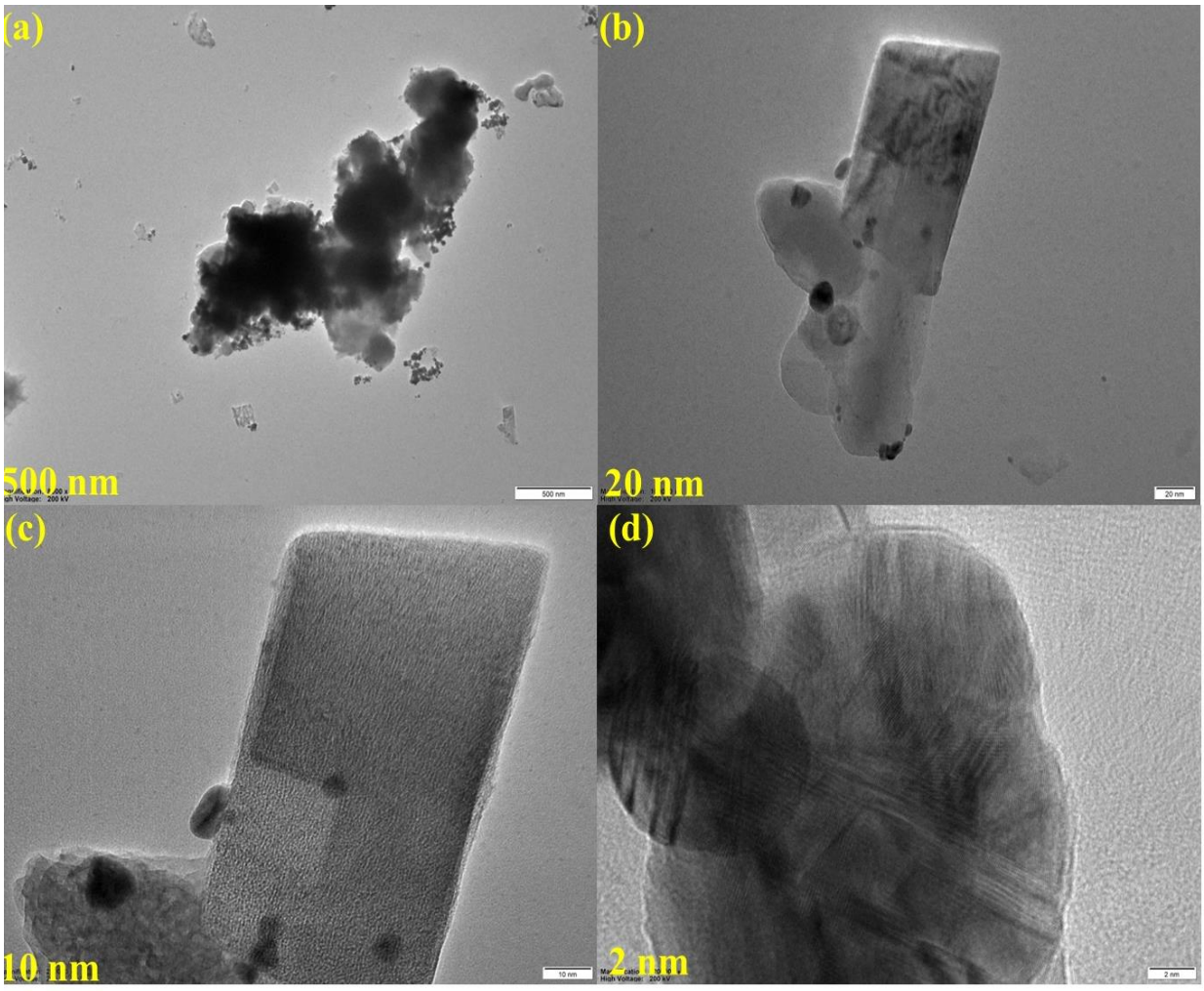

Fig.8: HR-TEM images of Ag-$CaTiO_3$

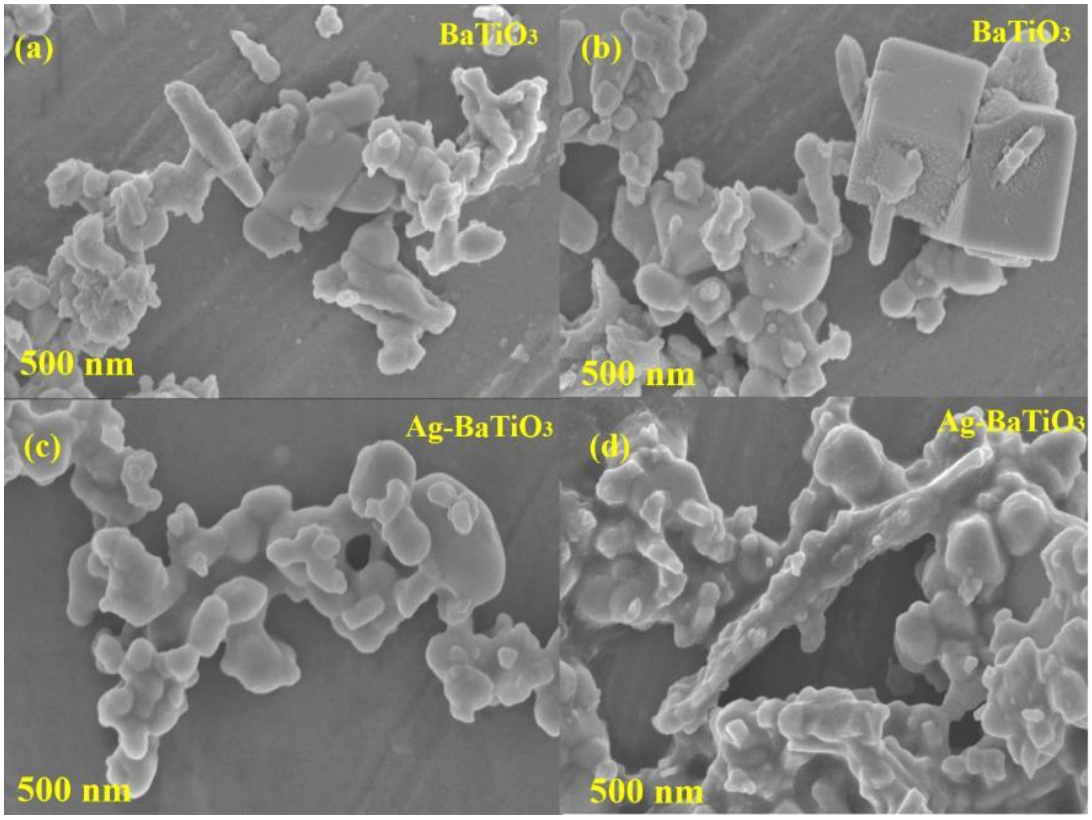

Fig.9: (a-b) FE-SEM images of $BaTiO_3$, (c-d) FE-SEM images of Ag-$BaTiO_3$.

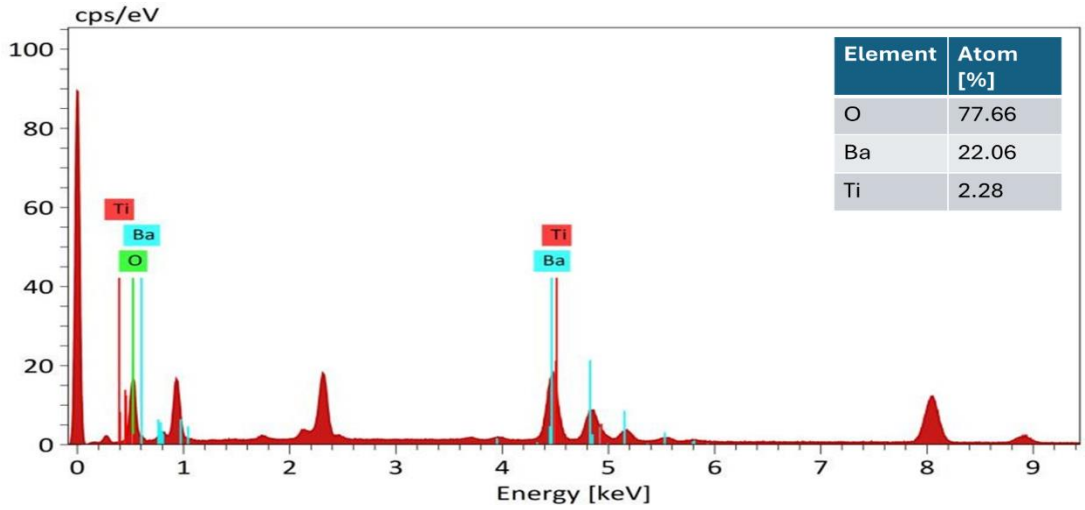

Fig.10(a): EDS analyis of $BaTiO_3$

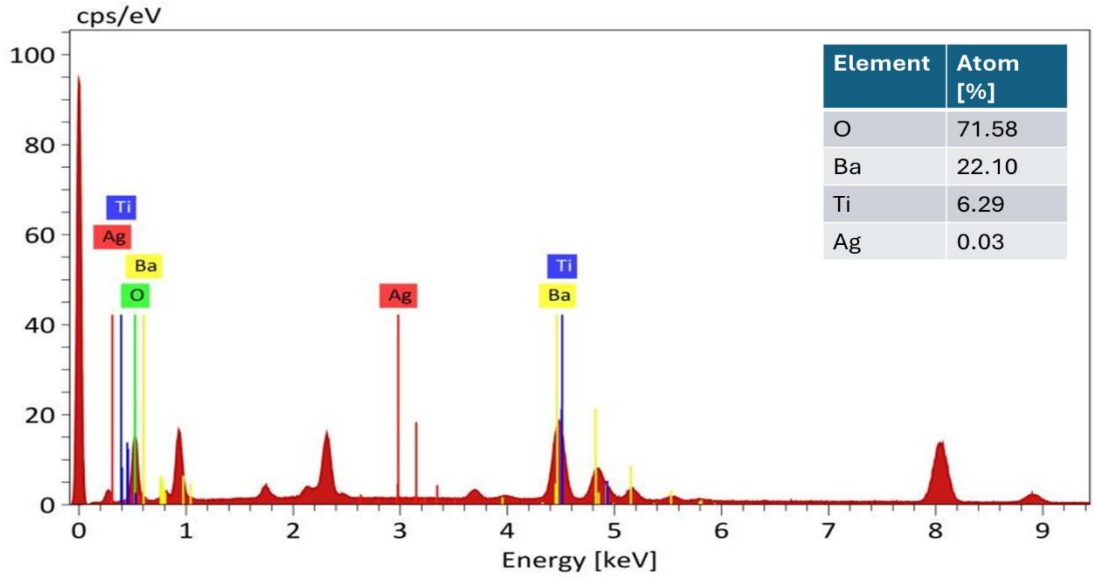

Fig.10(b): EDS analysis of 2wt% Ag loaded $BaTiO_3$.

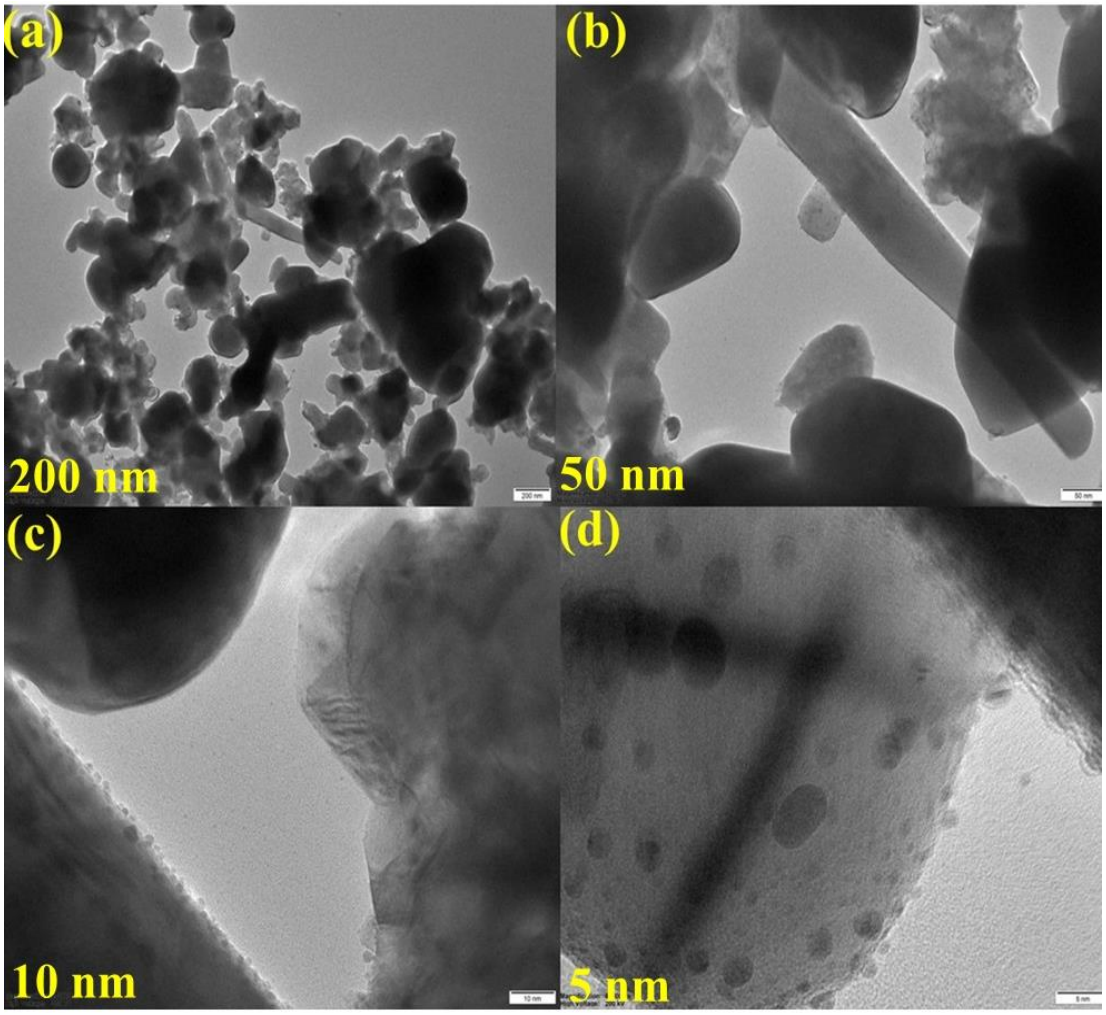

Fig.11: HR-TEM images of Ag-$BaTiO_3$.

3.3 Porosity and Surface Area Evaluation

Fig.12 represents the BET surface area of (a) $BaTiO_3$ nanocomposite (b) $CaTiO_3$ nanocomposite. According to the IUPAC classification, both samples' nitrogen (N2) adsorption-desorption isotherms showed type-IV Langmuir patterns with distinctive H3-shaped hysterisis loops, indicating their multilayer and mesoporous behavior. Pore size of both the samples is mainly that the catalysts have properties as of mesoporous material. Both samples and their composites have pore size between 5 to 12nm, hence supporting the idea that the catalysts are mesoporous materials. As depicted in Table 1, the Ag-$BaTiO_3$ composite (2.235 m^2/g) possesses less BET specific surface area in comparison with pristine BaTiO3 (3.15 m^2/g). This small drop is surface area is attributes to Ag NPs populating the pores on the surface of mesoporous $BaTiO_3$. As depicted in Table 2, The Ag-CaTiO3 composite (3.86 mg^2/g) have possesses BET surface area which 2 time less than that of 3,86 Ag-CaTiO3 (1.81 mg^2/g)).The enlargement observed in the various BET parameters could be ascribed to the incorporation of Ag with onto the $CaTiO_3$ surface, which would offer abundant active sites for the adsorption of contaminants, and facilitate rapid transportation of reactants and products hus, beneficial for attaining high photocatalytic activity. Fig. 13 shows the BJH curves for (a) $BaTiO_3$ (b) $CaTiO_3$

Table 1:

S. No.	Photocatalyst	Surface area	Total pore volume	Avergae pore diameter
1	$BaTiO_3$	3.15	6.806	8.1615
2	Ag-$BaTiO_3$	2.235	3.457	5.3161

Table 2:

S. No.	Photocatalyst	Surface area	Total pore volume	Avergae pore diameter
1	$CaTiO_3$	1.81	4.847	8.1562
2	Ag-$CaTiO_3$	3.86	5.578	6.6138

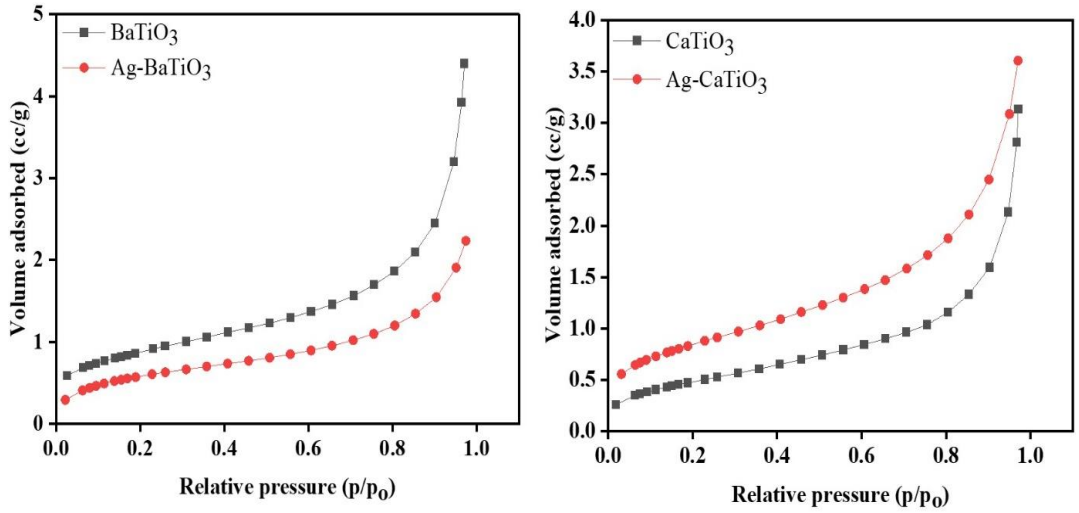

Fig.12: Nitrogen adsorption isotherns curves for (a) $BaTiO_3$ nanocomposites (b) $CaTiO_3$ nanocomposites.

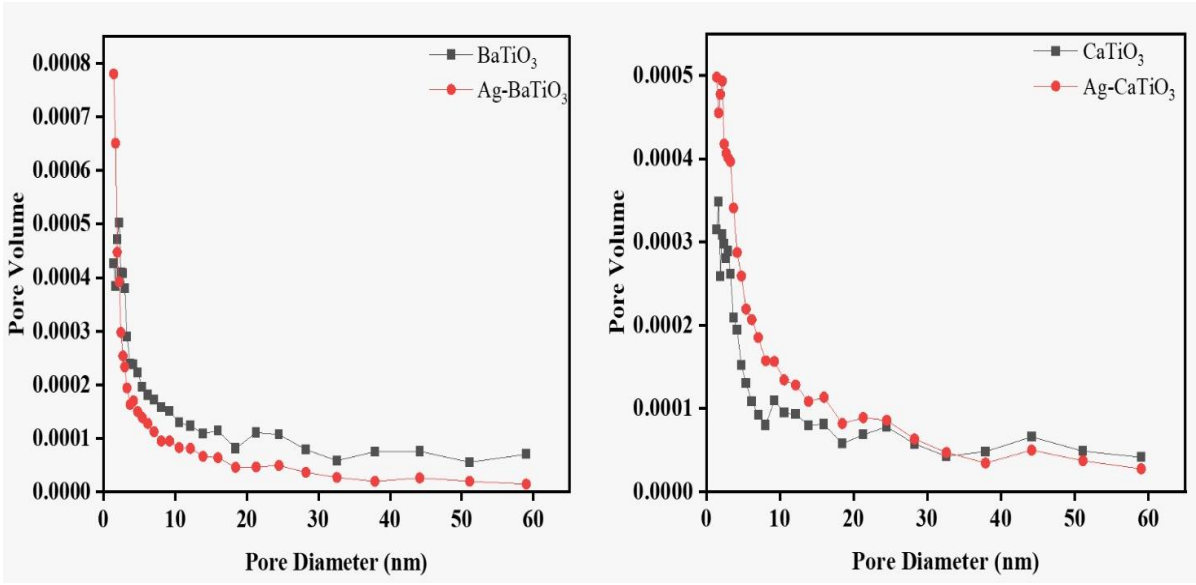

Fig.13: BJH graphs for (a) $BaTiO_3$ (b) $CaTiO_3$.

3.4 Optical and charge transfer specifications

UV-Vis Diffuse reflection measurements

UV-Vis diffuse reflectance spectra were carried out to determine the electronic properties of bare and silver-loaded composites. $BaTiO_3$ and $CaTiO_3$ exhibit peaks in the UV regions and no adsorption in the visible light range, which indicates that there is transition of electrons from the valence band to the conduction band. Doping of silver significantly increases their light absorption (red shift) property of bare silver towards the visible light region(400-800nm), which is attributed to the surface plasmon effect of Ag nanoparticles. LSPR bands were observed at 468nm for $BaTiO_3$ and 437nm for $CaTiO_3$. Color change from white to grey is also observed on the deposition of silver nanoparticles. Additionally, the band gap energy of a semiconductor is an important factor as it is associated with photocatalytic activity. The band gap energies of the samples were determinate through the Tauc relation, given by: $\alpha h\nu = A (h\nu - E_g)n$ where α = absorption coefficient, $h\nu$ = photon energy, A = constant, E_g = the band gap of the material and n is the exponent coefficient (n=2 for direct band gap and n=1/2 for indirect band gap). The exact band gap value was calculated by plotting graph between $(ahv)^{1/2}$ versus hv (for direct allowed transition) and $(ahv)^2$ versus hv(for indirect allowed transition). The Eg values of the $BaTiO_3$ and $CaTiO_3$, samples were designed to be 3.412 eV and 3.5 eV. The Eg values of Ag-$BaTiO_3$ and Ag-$CaTiO_3$ for direct band gap comes out to be 2.95eV {Fig.15 (b)} and 2.77eV. {Fig.15 (d)} The value of band gap decreases from 3.23eV o 2.95eV for $BaTiO_3$ and 3.22eV to 2.77eV for $CaTiO_3$ upon deposition of silver. The Ag deposited catalyst has a narrower band gap than the bare.

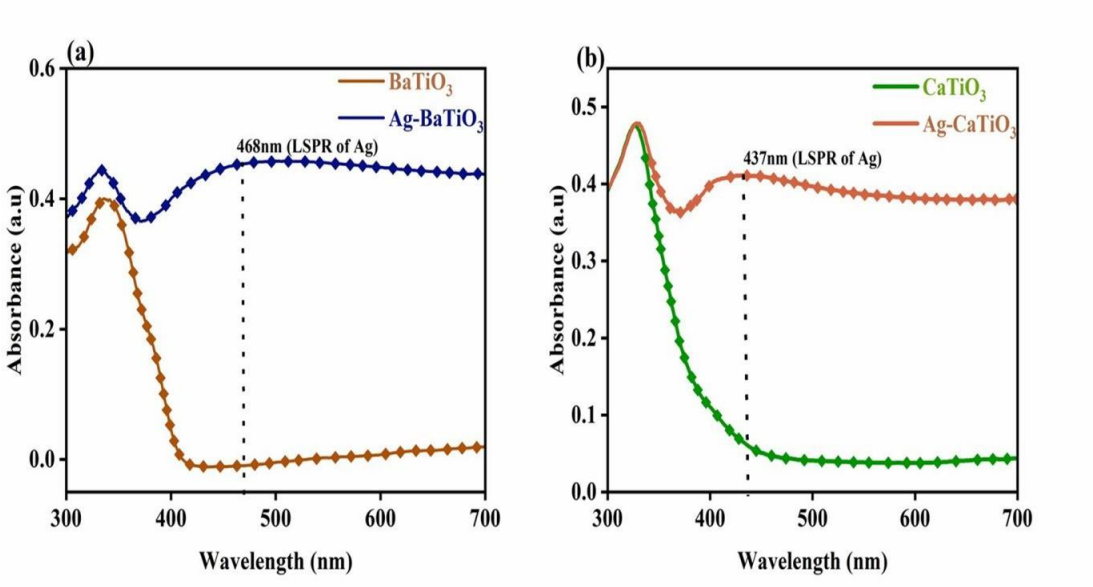

Fig.14: Diffuse reflectance spectra of (a) $BaTiO_3$ nanocomposites (b) $CaTiO_3$ nanocomposites.

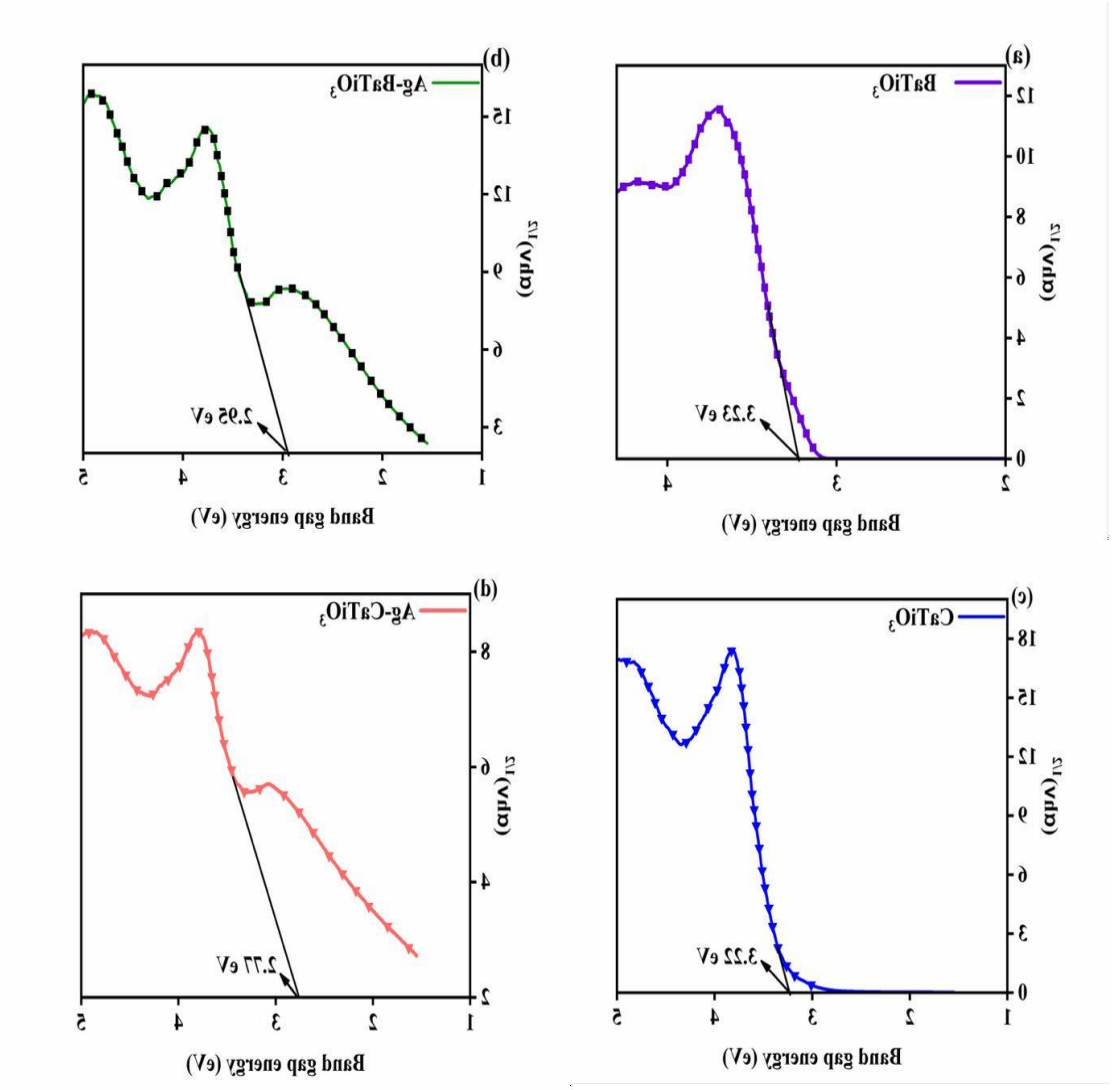

Fig.15: Tauc plots for direct allowed transition for (a-b) $BaTiO_3$ nanocomposites (c-d) $CaTiO_3$ nanocomposites.

Photoluminescence studies

PL spectroscopy was employed to evaluate the separation of charge carrier efficiency across several samples. PL strength is directly related to the rate of electron-hole pair recombination: higher recombination rates result in stronger PL signals, whereas lower rates result in weaker signals. Figure.16: (a) shows the PL spectra recorded at room temperature for $BaTiO_3$ and Ag-$BaTiO_3$ and (b) shows the PL spectra recorded at room temperature for $CaTiO_3$ and Ag-$CaTiO_3$. $BaTiO_3$ samples show peak at 423nm, 468nm and 551nm, whereas $CaTiO_3$ samples show peak at 423nm, 468nm and 550nm. The peak at 423nm ascribes to near band emission (NBE),

whereas the latter peaks at 468 and 550nm corresponds to deep level emissions (DLE). The NBE peaks in UV regions mainly occurs due to recombination of charge carriers formed by excitation of radiation with energy equal or greater than the bandgap energy. The other two DLE peaks in the visible region are associated with intrinsic defects such as oxygen vacancies (V_o), Ti vacancies (V_{ti}) or surface defects[38]. The highest PL intensity, which shows a high rate of recombination and reduced efficiency of photoinduced charge carrier separation. The intensity of PL peaks decreases, upon the introduction of Ag nanoparticles. This PL quenching is due to the effective migration of electrons from the bare to the surface of deposited silver for electron transport. Increasing the silver content beyond 2% leads to an increase in PL intensity. As excess metal can increase the rate of recombination and decrease photocatalytic effectiveness.

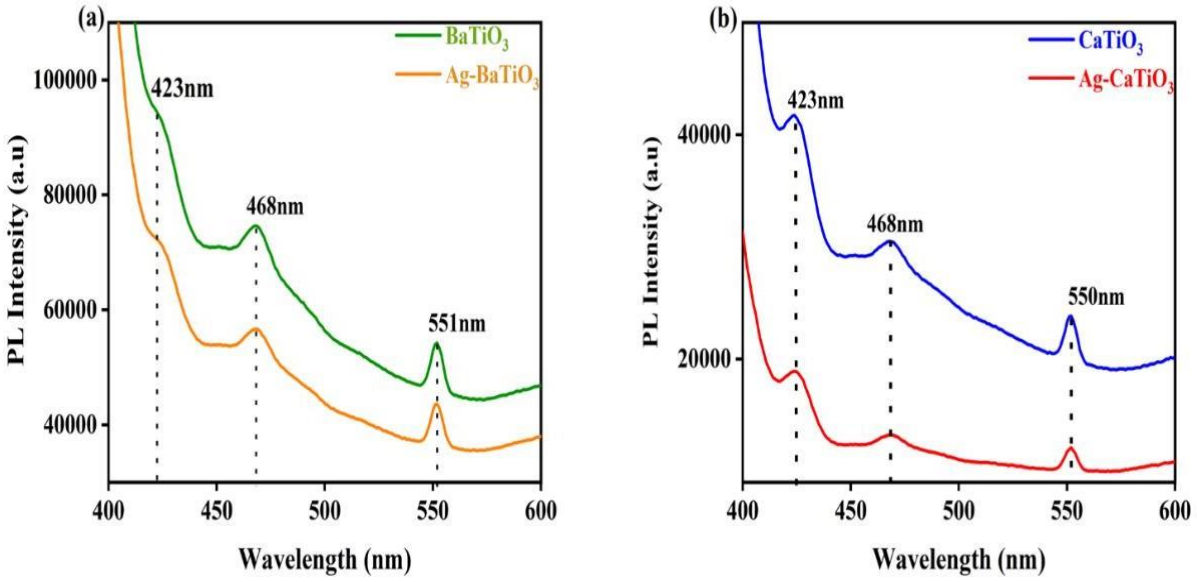

Fig.16: Photoluminescence spectra of (a) $BaTiO_3$ nanocomposites (b) $CaTiO_3$ nanocomposites.

3.5 Photocatalytic activity

3.5.1 Photocatalytic degradation

The light-driven catalytic efficiency of the Ag- $BaTiO_3$ and Ag-$CaTiO_3$ nanocomposite was initially assessed by investigating the Visible light and sunlight-induced breakdown of the cationic dye methylene blue (MB). To provide a comparison, Methylene blue was removed from the bare $BaTiO_3$, $CaTiO_3$, Ag-$BaTiO_3$ and Ag-$CaTiO_3$ composites. In the nonexistence of a photocatalyst, just 11% of methylene blue is destroyed after 1h of direct sunlight exposure, suggesting its remarkable steadiness. Following 2h of dark adsorption, the adsorption effectiveness of several composites was computed: $BaTiO_3$: 42.5%; Ag-$BaTiO_3$: 52.7% $CaTiO_3$: 42.3% Ag-$CaTiO_3$: 45.19%. Fig.17(a-b) shows degradation efficiency of methylene blue by $BaTiO_3$ nanocomposites under visible light; (c-d) shows degradation efficiency of methylene blue by $CaTiO_3$ nanocomposites under visible light. Fig.18(a-b) shows degradation efficiency of methylene blue by $BaTiO_3$ nanocomposites under sunlight. (c-d) shows degradation efficiency of methylene blue by $BaTiO_3$ nanocomposites under sunlight. Ag loaded nanocomposites exhibits higher adsorption towards methylene blue than unmodified bare nanocomposites, and when Ag is deposited onto the surface of $BaTiO_3$ and $CaTiO_3$, its adsorption capacity increases. After 2.5h of sunlight exposure, the nanocomposites degradation efficiency advances according to the outlined progression: Ag- $BaTiO_3$ (99.2%) > $BaTiO_3$ (55.6%) in comparison to 4h visible light irradiation Ag- $BaTiO_3$(95.19%) > $BaTiO_3$(85.86%). {Fig.19 (a-b)}The 2.5-hour exposure to sunlight resulted in higher degradation efficiencies for Ag-$BaTiO_3$, while $BaTiO_3$ showed lower efficiency compared to the 4-hour of visible light exposure. Similarly, for $CaTiO_3$ after 1h of light exposure, the nanocomposites degradation efficiency advances according to the outlined progression: Ag-$CaTiO_3$ (99.4%) > $CaTiO_3$ (80.8s6%) in comparison to 1.5h visible light irradiation Ag-$CaTiO_3$ (97.9%)> $CaTiO_3$ (89.2%). {Fig.16 (c-d)}. Thus, the Ag loaded nanocomposites (Ag-$BaTiO_3$ and Ag-$CaTiO_3$) eliminates methylene blue to more extente, which is consistent with previous characterization findings. Furthermore, utilizing pseudo- first-order rate kinetics, the related reaction rate constants (k) were Determined through numerical analysis, $\{\ln(Ct/C_0) = -kt\}$[39] here C_0 is the initial concentration of MB dye, C_t is its concentration at the time (t), and k denotes the rate constant (min^{-1}). Figure. 9 shows the $\ln(C_t/C_0)$ readings for the prepared samples. Fig.20(a) shows rate constant of $BaTiO_3$($0.72403min^{-1}$) and Ag-$BaTiO_3$($0.4755min^{-1}$) under visible light, (b) rate constant of $BaTiO_3$($1.30716min^{-1}$) and Ag-$BaTiO_3$($0.89509min^{-1}$) under sunlight (c) rate constant of $CaTiO_3$($0.04106min^{-1}$) and Ag-$CaTiO_3$($0.02548min^{-1}$) under visible light (d) rate constant of

$CaTiO_3$(0.08098min^{-1}) and Ag-$CaTiO_3$(0.04333min^{-1}) The Ag loaded photocatalysts had a high methylene blue degrading rate constant , which is nearly 3 times greater than that of bare photocatalysts. .The Ag-$BaTiO_3$ and Ag-$CaTiO_3$ nanocomposite showed a markedly greater decline after 2.5h and 1h of sunlight exposure . The comprehensive reducing pattern seen in the methylene blue spectral analysis demonstrates the superior photocatalytic efficiency of Ag-$BaTiO_3$ and Ag-$CaTiO_3$ suggesting that the Ag loading helps enhance the photocatalytic activity of $BaTiO_3$ and $CaTiO_3$. The experimental results show that adding Ag on the surface of $BaTiO_3$ and $CaTiO_3$ considerably improves its degraded performance. These metallic coatings operate as electron accumulation sites, catching photo-excited electrons from the $BaTiO_3$ and $CaTiO_3$ surfaces, preventing recombination of electron holes pairs. This process enhances the production of highly reactive electrons and superoxide radical anions (.O2 -), which are essential for successfully degrading methylene blue dye. In summary deposition of silver nanoparticles enhances the photocatalytic degradation efficieny and in comparison to the light source i.e visible light and sunlight, sunlight is more effective for the degradation of methylene blue dye.

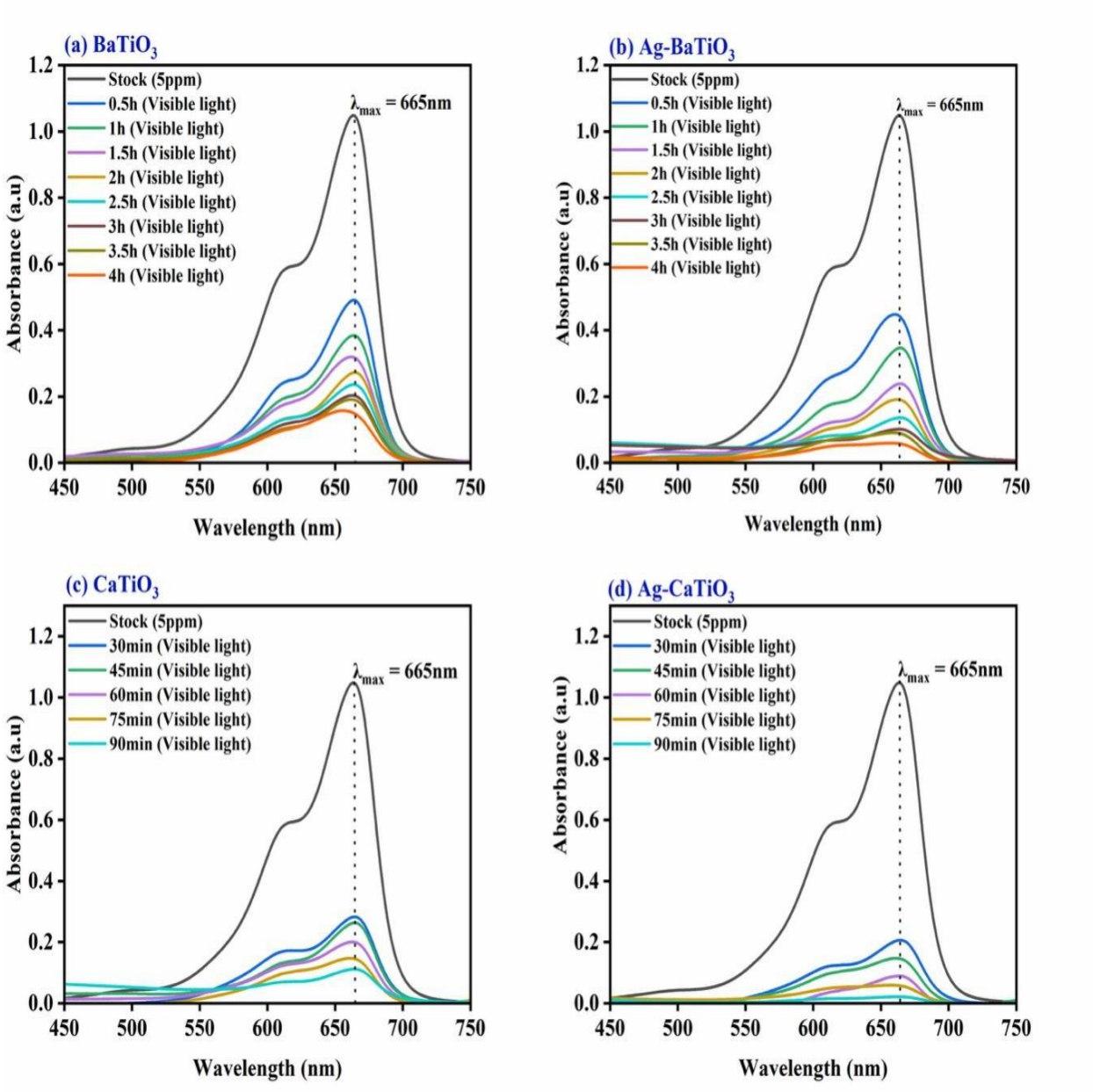

Fig.17: Photocatalytic degradation of methylene blue under visible light by (a-b) $BaTiO_3$ nanocomposites (c-d) $CaTiO_3$ nanocomposites.

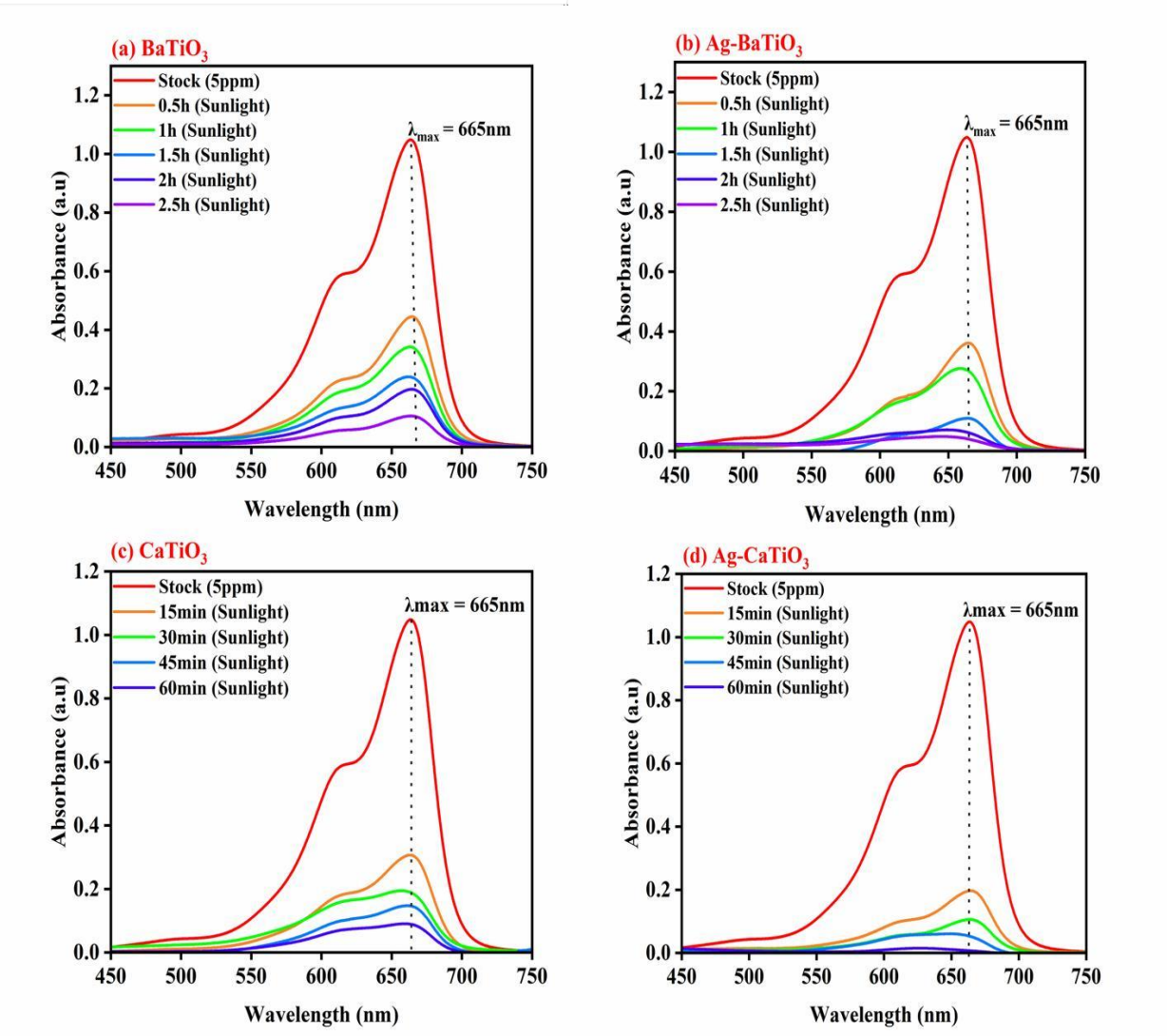

Fig.18: Photocatalytic degradation of methylene blue under sunlight by (a-b) $BaTiO_3$ nanocomposites (c-d) $CaTiO_3$ nanocomposites.

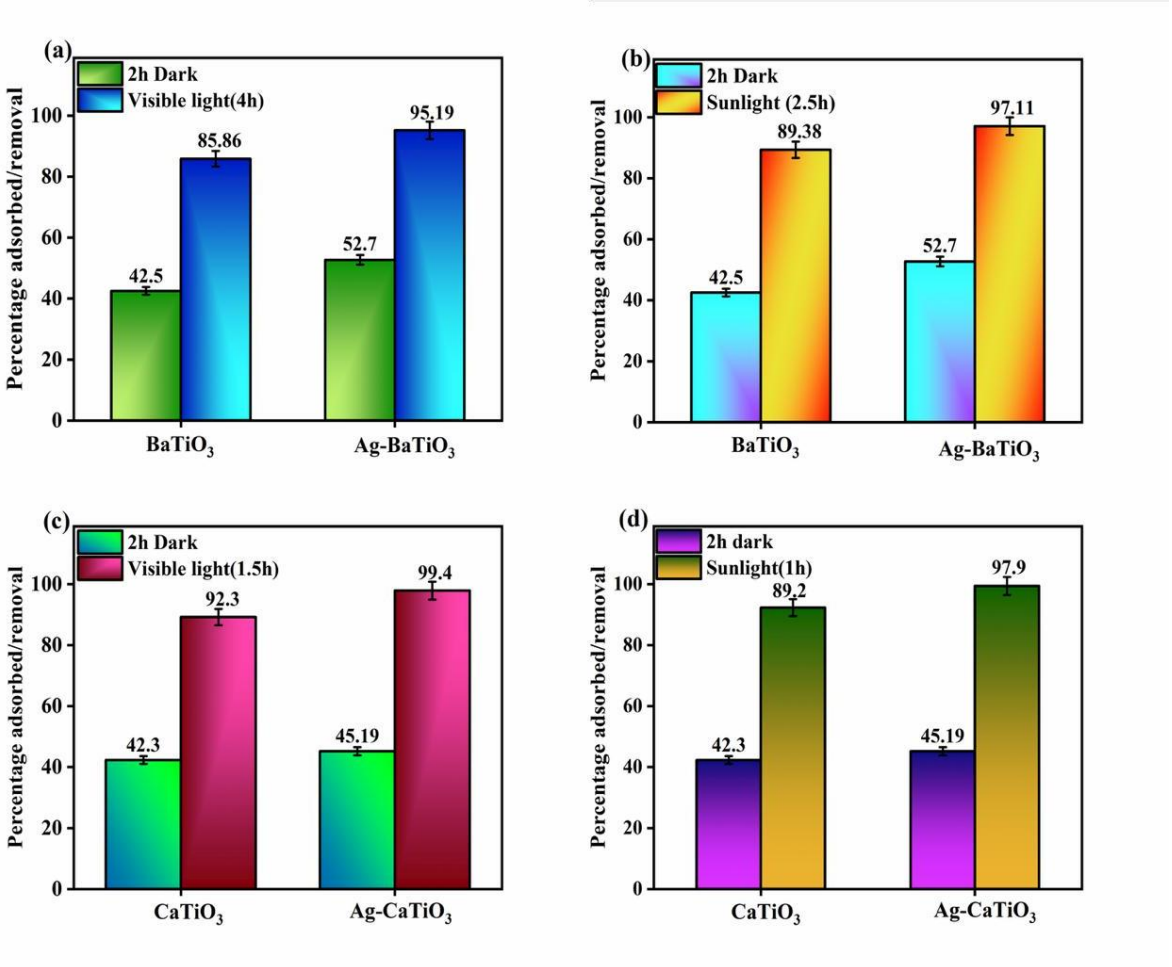

Fig.19: Photocatalytic degradation of methylene blue by (a-b) $BaTiO_3$ nanocomposites (c-d) $CaTiO_3$ nanocomposites.

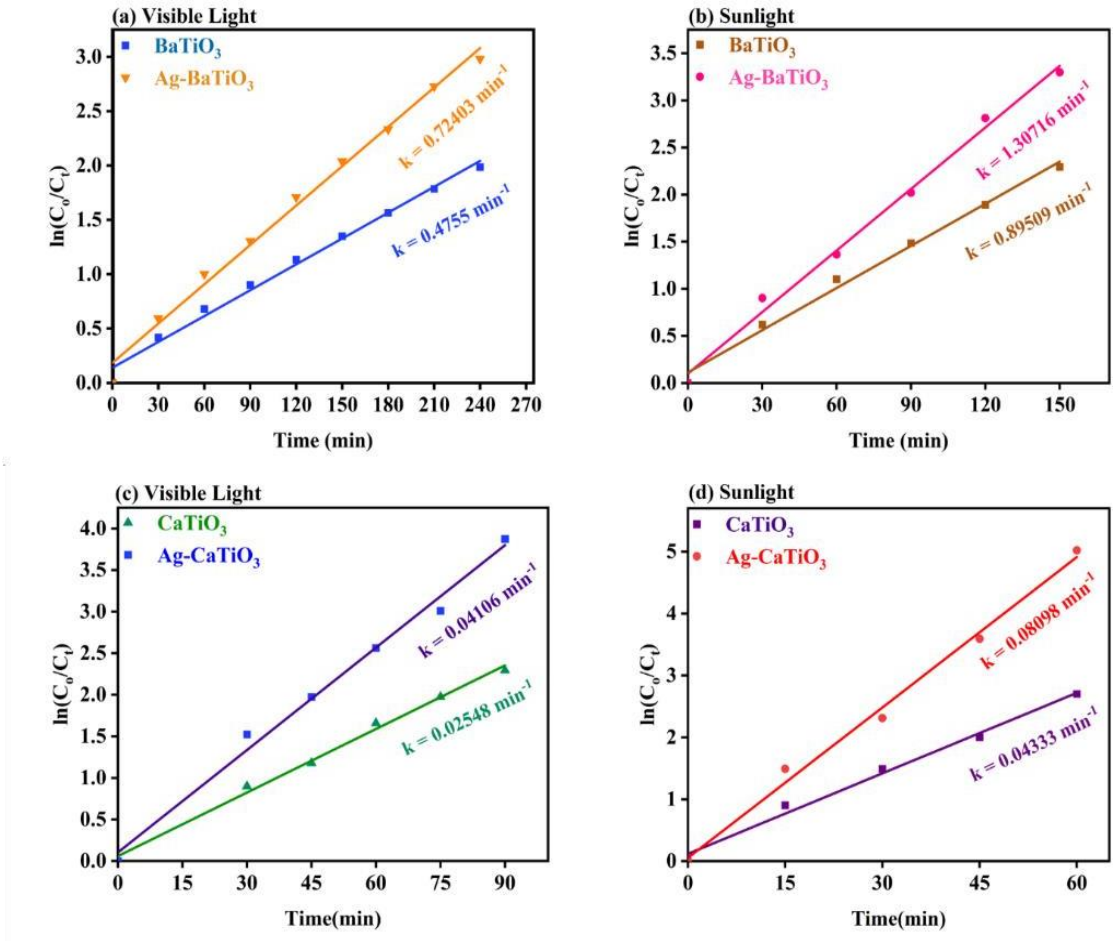

Fig.20: Time course kinetic plot of pseudo first order reaction of (a-b) $BaTiO_3$ nanocomposites (c-d) $CaTiO_3$ nanocomposites.

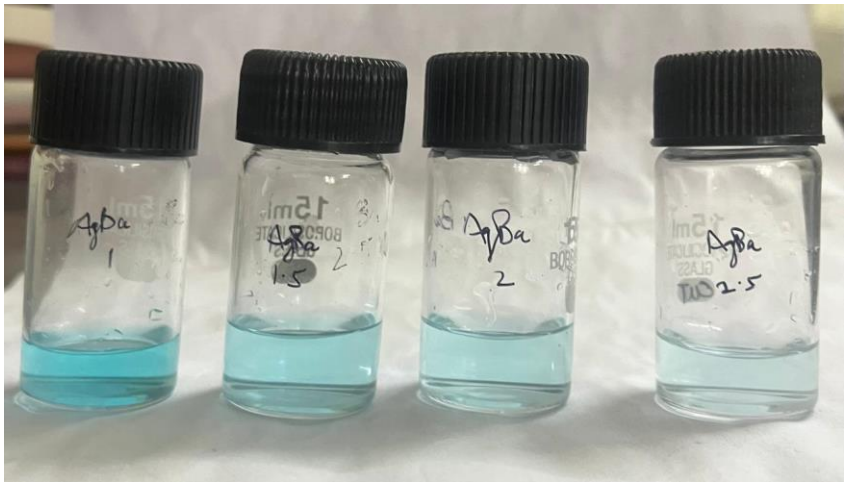

Fig.21: Degradation of Methylene Blue by Ag-$BaTiO_3$ under visible light.

Fig.22: Degradation of MB dye by Ag-$CaTiO_3$ under sunlight

2.5.2 Effect of visible/sunlight illumination: Under ideal conditions, relative studies assessed photocatalytic activity using various light sources, including visible, and natural sunlight. As shown in Fig.14, dye is degraded at an efficiency of 85.86% under visible irradiation and 89.38% under natural sunlight for $BaTiO_3$. Using the Ag-$BaTiO_3$ nanocomposite under natural sunlight resulted in the removal efficiency of 97.11%. According to Fig., pollutants degraded at an efficiency of 89.2% under visible irradiation and 92.3% under natural sunlight for $CaTiO_3$. Notably, using the Ag-$BaTiO_3$ nanocomposite under natural sunlight resulted in the best removal efficiency of 99.4%. Natural sunlight consistently outperformed visible light in terms of pollutant degradation efficiency for both $BaTiO_3$ and $CaTiO_3$. The incorporation of Ag into the $BaTiO_3$ and $CaTiO_3$ structures significantly enhanced their degradation efficiencies under natural sunlight. The Ag-$CaTiO_3$ nanocomposite achieved the highest degradation efficiency of 99.4% under natural sunlight, making it a promising candidate for practical applications. These findings highlight the superior 24 effectiveness of natural sunlight in pollutant degradation in conjunction with the proposed photocatalyst. Thus, natural sunlight has a significant advantage over non-natural light sources for Contaminant breakdown.

3.6 Mineralization of dye by TOC measurement

Total Organic Carbon (TOC) testing was utilized to assess the effectiveness of mineralization of pollutant molecules during photocatalysis, as mineralization is the ultimate goal of pollutant treatment. TOC values represent the amount of organic carbon dissolved in the aqueous solution. A decrease in TOC concentration indicates the level of mineralization achieved upon completion of the reaction. In this study, TOC analysis was conducted at the beginning and end of the photodegradation process to determine the extent of Methylene blue dye mineralization facilitated by the fabricated Ag-$CaTiO_3$ photocatalyst. The TOC values were measured at the start and end of the photodegradation process. The reduction in TOC concentration was used to determine the level of mineralization achieved. This analysis provides insight into the effectiveness of the photocatalyst in breaking down the organic pollutant into inorganic compounds. The findings demonstrate that the TOC values of Methylene blue dye decreased from 41.3 to 22 mg/l after 60 minutes of direct sunlight exposure, representing a 46.8% TOC reduction. The Ag-$CaTiO_3$ photocatalyst shows promise in breaking down methylene blue pollutants, as evidenced by the decrease in Total Organic Carbon (TOC) values. While the UV-Vis spectrophotometer results indicate high degradation efficiencies, they also reveal that mineralization activity is slightly lower. This discrepancy can be attributed to the formation of intermediate products, which were identified through High-Resolution Mass Spectrometry (HRMS) studies. Although complete mineralization of these intermediates is achievable, it may require prolonged exposure to sunlight.

Mineralization(%) = $Oiitil - Ofil$/TOCinitialX100%

Where, $TOC_{initial}$ and TOC_{final} values are the total organic carbon content of methylene blue (mg/L) before and after the degradation process, respectively.

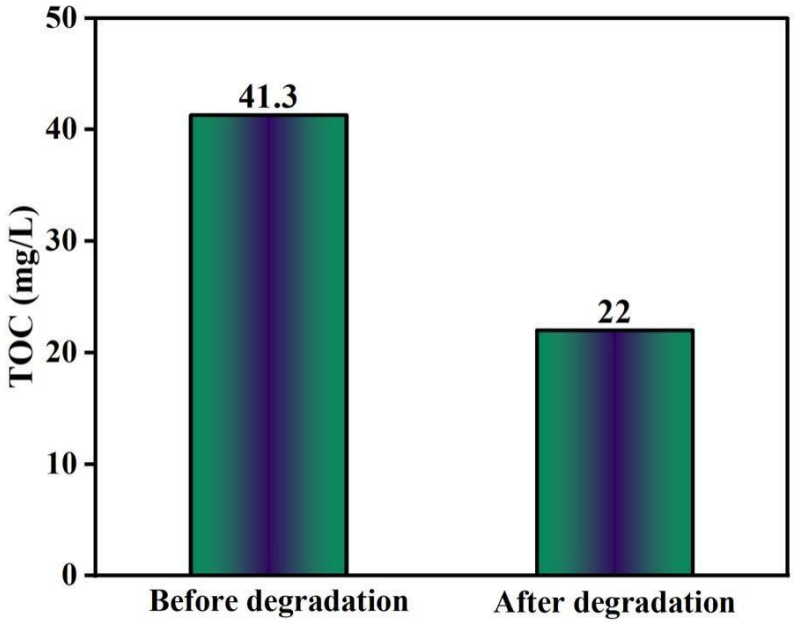

Fig. 23: TOC of Ag-$CaTiO_3$.

3.7 Scavengers studies

To identify the active species in Ag-$BaTiO_3$ and Ag-$CaTiO_3$ for photocatalytic degradation, radical capture studies were conducted. Various scavengers (EDTA, benzoquinone, IPA) were selected for the quenching of photoproduced holes(h+), O2.- and. OH radicals. The conditions were kept identical as for the free radical trapping and degradation experiments. As shown in Fig.24 , the photo removal effectiveness of Methylene blue was decreased in the presence of scavengers with the significance order following benzoquinone> IPA>EDTA which indicates that .OH and h+ are the primary contributors for the degradation process of MB, whereas O2.- plays a minor role. On addition of benzoquinone degradation process was affected only up to a low extent, showing that superoxide radical anions play insignificant role the degradation process. The degradation efficiency was affected largely on addition of IPA and EDTA, showing that .OH radicals and h+ are the primary active species for the degradation of mb dye. Results obtained concludes that h+ is the important primary reactive species in the degradation process.

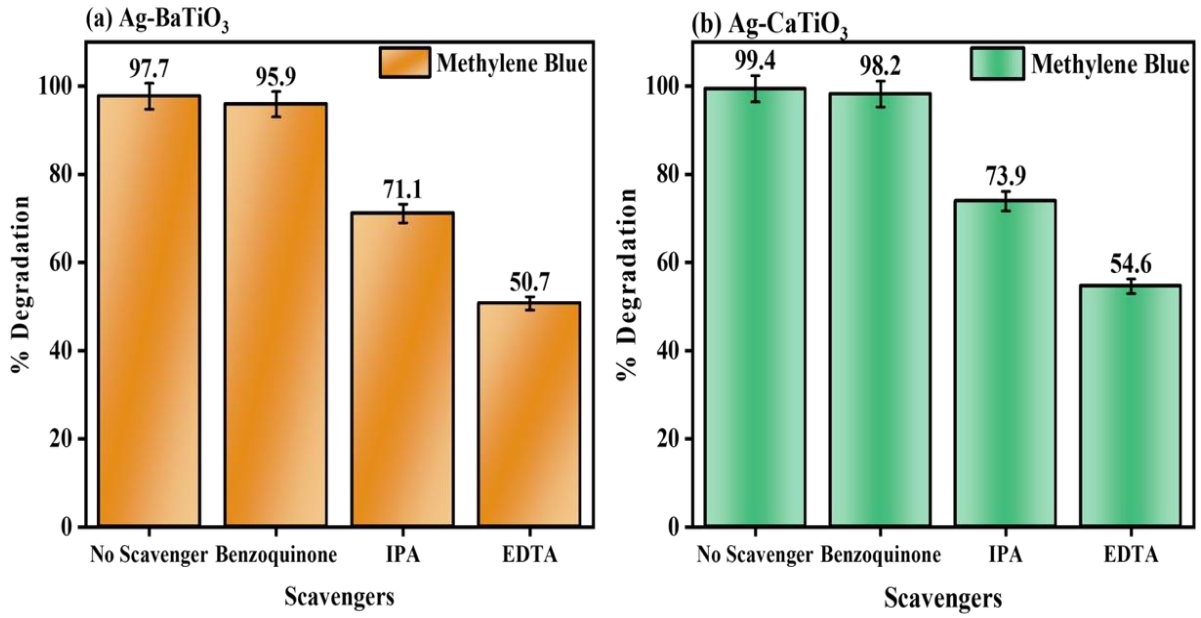

Fig.24: Impact of set of scavengers on Methylene blue degradation (a) Ag-$BaTiO_3$ (b) Ag-$CaTiO_3$.

3.8 Photocatalytic degradation pathways

(a)

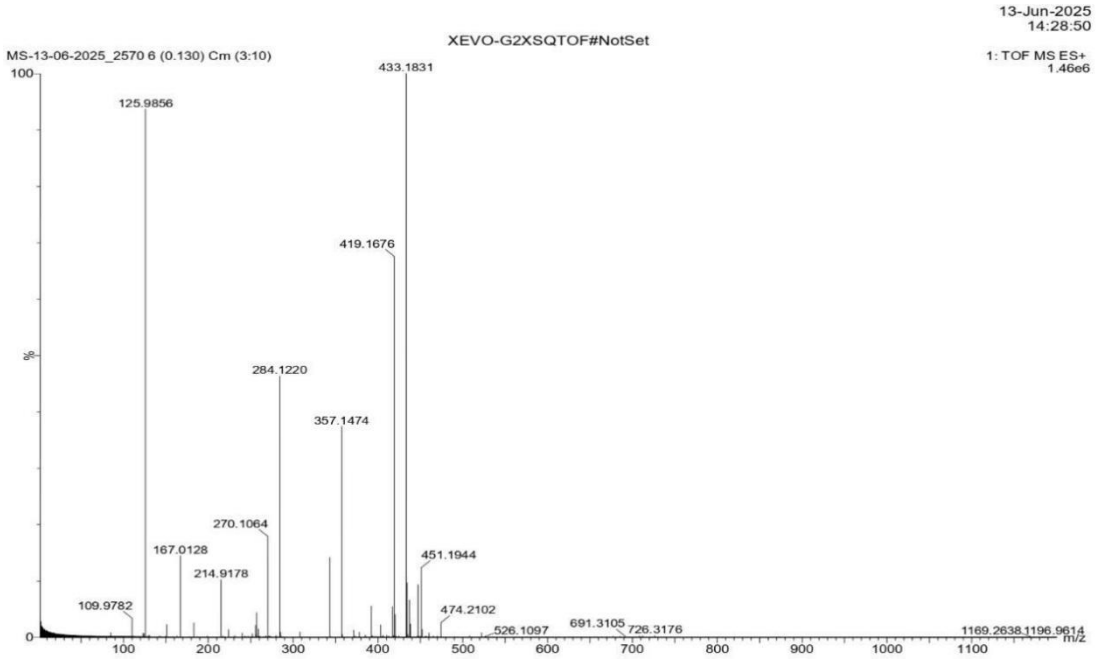

(b)

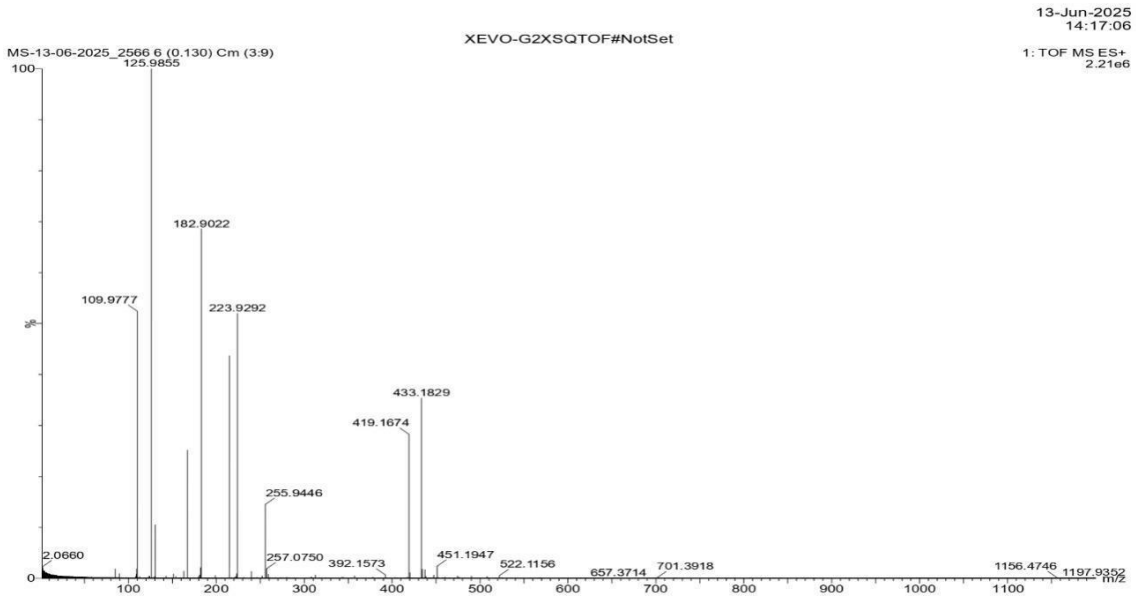

Fig.25: HRMS data of $BaTiO_3$ photocatalyst when MB degraded (a) 76.8% (b) 97.11%.

Based on HRMS data, the photocatalytic degradation pathway of methylene blue could be determined. The mass spectra of methylene blue (m/z = 284) degraded by 76.87% and 97.11% are shown in Fig. 25(a) and (b), respectively, to further determine the degradation intermediates' compositions. For **Pathway 1:** The intermediate product with a mass-to- charge ratio (m/z) of 284 is due to the MB pollutant. Besides, the m/z ratios produced with the photocatalytic process were 284, 270, 256 219, and 105. According to the previous reports and the exploration of the results, the conceivable photocatalytic route was exhibited in Fig. 26. The MB pollutants were decayed to the intermediate product through a demethylation reaction by the intermediate product of m/z ratio of 270. The above intermediate was converted to the intermediate of m/z ratio of 256 (Observed peak= 255 + H+) via either demethylation or deamination reaction which is an obvious implication of the photocatalytic of MB pollutants. The following pathway, after the desulfurization reaction, the next step is through shortening and ring opening. The m/z ratio is 109 corresponding to 1,4-butanedione, etc. These small molecules are transformed into CO_2 and H_2O eventually[40].

Pathway 2: Destroying the nitrogen-sulfur heterocycle through an h+ attack is one of the possible degradation pathways (path 1). Intermediate product A is produced when the N-S heterocycle is cracked by the attack of h+ to N14 and S13. Meanwhile a benzenesulfonic derivative is generated as intermediate product B from the ring opening of the N-S heterocycle during the oxidation. Then B is attacked preferentiallsy by h+ and ·OH to generate intermediate product C. C is easy to attack by h+, and the amino group is removed to form intermediate product D. As the degradation progresses, the benzene ring of intermediate product D is opened under combined action of h+ and ·OH, and MB and degradation products are eventually mineralized to form simple inorganic molecules, like NO_3^-, SO_4^{2-}, CO_2 and H O[41].

Pathway 3: As shown in fig.: 26, HO˙ radicals attack the C–S+ C functional group in MB at m/z = 303.(Observed dehydrated peak at [284+ Na+]) The electrophilic attack of HO˙ involved the free doublet of heteroatom S, causing its oxidation state to change from −2 to 0. However, the transformation from C–S+ C to C–S(O)–C requires conservation of the double bond, which induces the opening of the central aromatic ring containing both heteroatoms (S and N). The origin of the H atoms necessary for C-H and N-H bond formation is proposed to be from proton reduction by photogenerated electrons, as this is already been observed in MB dehydrogenation.With further degradation, the main by-products of the degradation process are 2-aminophenol, 2-amino-5-(methylamino)hydroxybenzenesulfonic acid (Observed reduced peak at 214) and 2-amino-5-(N-methylformamido)benzenesulfonic acid (Observed peak at [223 + Li+]), as shown by mass spectrometry analysis which gives m/z values of 109, 218 and 230, respectively. Finally, the intermediates could be further decomposed into small molecules, like carbon dioxide and water Finally, the d into small molecules, like carbon

dioxide and water.

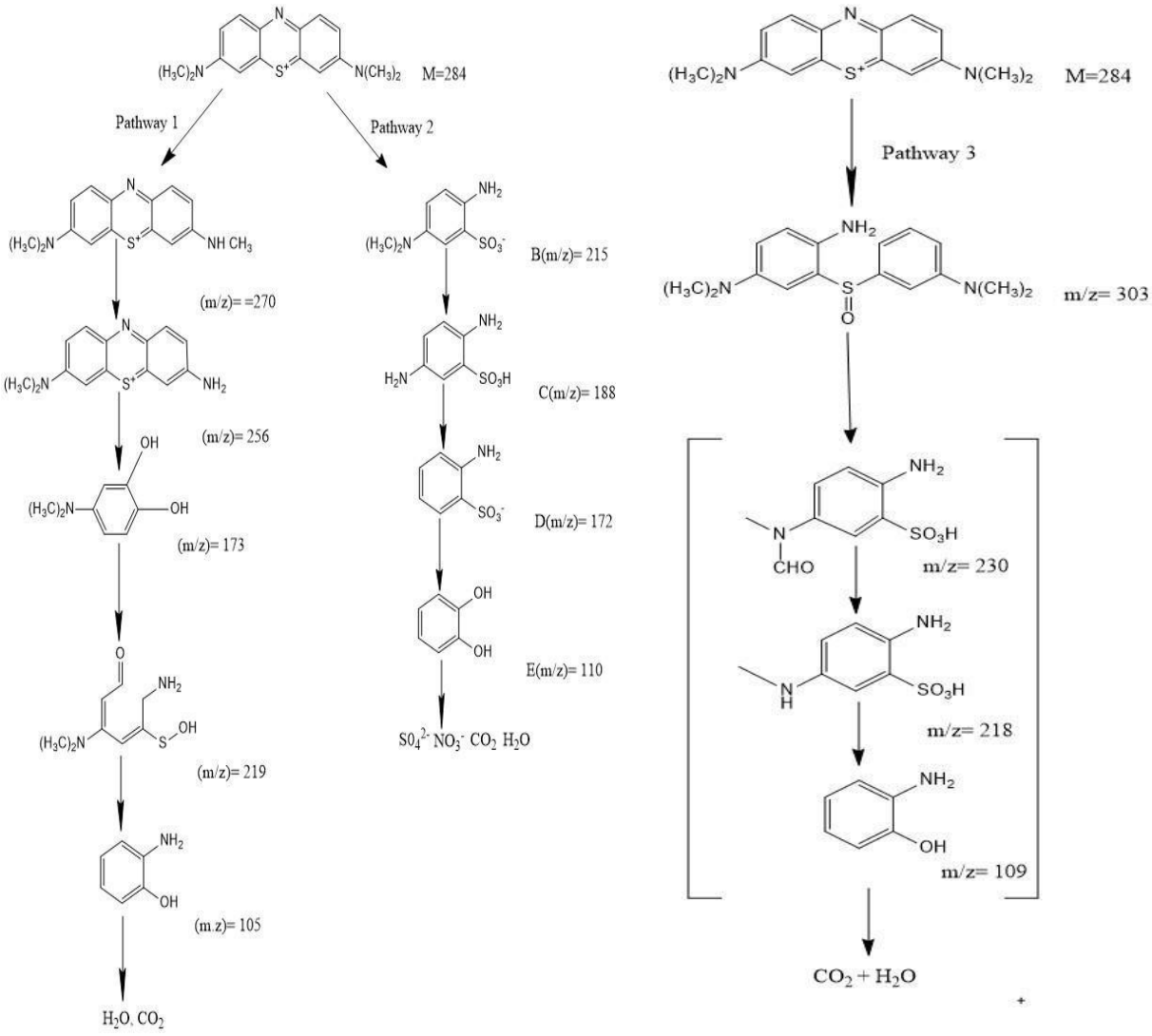

Fig.26: Degradation pathway mechanism of Methylene blue dye by Ag-$BaTiO_3$ photocatalyst under sunlight.

3.9 Possible Degradation mechanism

When sunlight hits $BaTiO_3$ and $CaTiO_3$, it excites electrons from the valence band to the conduction band, creating holes in the valence band. These electrons and holes are crucial for the subsequent reactions. The excited electrons and holes interact with oxygen and water molecules adsorbed on the surface of the photocatalyst. This interaction leads to the formation of reactive oxygen species (ROS) like superoxide radical anions (·O2─) and hydroxyl radicals (·OH). These ROS are highly oxidative and can effectively degrade organic

pollutants like Methylene blue dye. Silver has a lower redox potential compared to the conduction band potential of $BaTiO_3$ and $CaTiO_3$. This allows the photoexcited electrons to flow quickly from the photocatalyst to the Ag surface. Essentially, Ag acts as an electron sink, facilitating the separation of electron-hole pairs and preventing their recombination. This enhances the efficiency of the photocatalytic process. The overall reactions during photocatalysis under sunlight, with Ag-deposited ($BaTiO_3$) photocatalyst are depicted below:

$$Ag + hv \rightarrow Ag\ (h^+ + e-) \quad (1)$$

$$BaTiO_3 + hv \rightarrow BaTiO_3\ (h_+ + e-) \quad (2)$$

$$Ag\ (e-) + BaTiO_3 \rightarrow BaTiO_3\ (e-) + Ag \quad (3)$$

$$BaTiO_3\ (e-) + O_2 \rightarrow BaTiO_3 + {\cdot}O_2^- \quad (4)$$

$$Ag\ (e-) + O_2 \rightarrow Ag + .O_2^- \quad (5)$$

$$O2^- + H^+ \rightarrow OOH \quad (6)$$

$$OOH \rightarrow O_2 + H_2O_2 \quad (7)$$

$$H_2O_2 + (e-) \rightarrow OH + {}^-OH \quad (8)$$

$$Ag\ (h^+) + {}^-OH \rightarrow OH \quad (9)$$

$$BaTiO_3\ (h+) + {}^-OH \rightarrow OH \quad (10)$$

$$O2^-/\ OH + MB \rightarrow CO_2 + H_2O + \text{degradation products} \quad (11)$$

This transport mechanism in the metal-loaded photocatalyst is anticipated to reduce charge carrier recombination, greatly enhancing photocatalytic performance

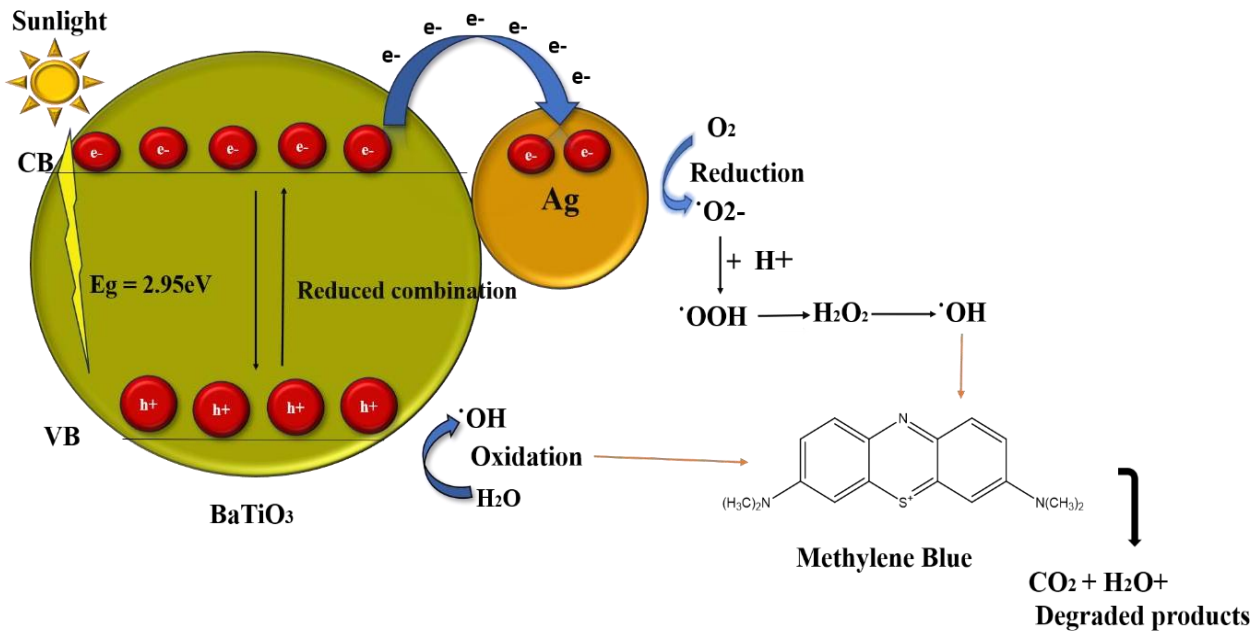

Scheme 4: Mechanism of Methylene Blue degradation under sunlight.

3.10 Recyclability Studies

A series of recycling tests were performed using Ag-$BaTiO_3$ and Ag-$CaTiO_3$ for the degradation of MB dye. For evaluating the reusability of composites photocatalytic activity was assessed for 5 consecutive cycles. For each cycle, the photocatalyst was retrieved via centrifugation from the previous one. It was then cleaned and dried. According to Figure, the degradation efficiency of the MB dye dropped by just small in case of Ag-$BaTiO_3$ and for Ag-$CaTiO_3$. The reduction in the degradation process from to and from to can be due to loss of catalyst during the separation and recycling process. In summary, The Ag-$BaTiO_3$ and Ag-$CaTiO_3$ composites demonstrate excellent degradation performance, good renewability, and robust photostability, making them suitable for practical applications in wastewater treatment. The minimal reduction in degradation efficiency after multiple cycles highlights the stability and potential for long-term use of these photocatalysts.

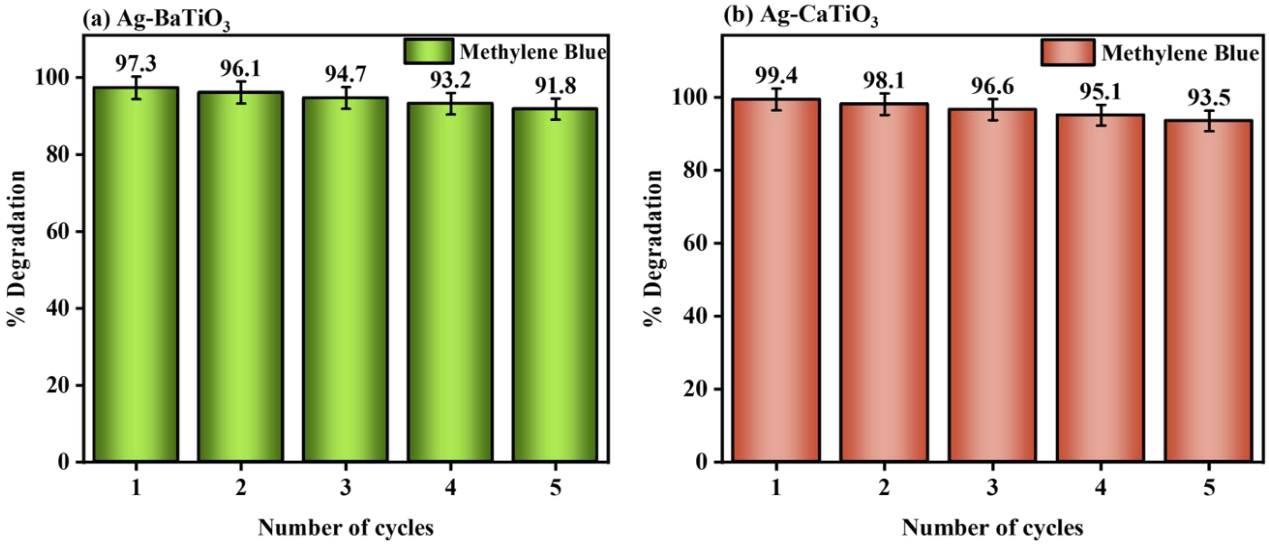

Fig.27: Recyclability studies (a)Ag-$BaTiO_3$ (b) Ag-$CaTiO_3$.

4. CONCLUSION

$BaTiO_3$ and $CaTiO_3$ were synthesized using the hydrothermal method and were loaded with metal Ag to improve its photocatalytic properties. The successful fabrication of the samples was confirmed by multiple analyzing techniques such as DRS, FE-SEM, HR-TEM, XRD and PL analyses. FE-SEM and HR-TEM images confirm that Ag was efficiently deposited on the surface of $BaTiO_3$ and $CaTiO_3$. The synthesized samples were used to study the degradation of Methylene blue dye using sunlight to evaluate the photocatalytic efficiency of the synthesized samples [105]. The photocatalysts exhibited the maximum photocatalytic efficiency and rate constant for Ag-$CaTiO_3$. The composite was found to photocatalytically degrade pollutants by natural sunlight according to PL, BET, and UV-visible DRS tests occurring at a lower electron-hole recombination rate, large surface area, and appropriate band gap. Different parameters including reaction kinetics, type and wavelength of light sources, scavenger analysis, and reuse sof the photocatalyst were also investigated in the study for photocatalytic degradation. Using trapping experiments, h^+ was determined to be the predominant species responsible for degradation of the pollutants. The recyclability of the composite was also excellent for up to 5 cycles. In conclusion, the Ag-$BaTiO_3$ and Ag- $CaTiO_3$ catalysts exhibited significant depletion activity for organic pollutants under low consumption in natural sunlight, which is a promising feature and ready to apply for scale-up industrial wastewater treatment due to its low cost, ease, and environmentally friendly.

References:

[1] K. M. Reza, A. Kurny, and F. Gulshan, "Parameters affecting the photocatalytic degradation of dyes using TiO2: a review," Jul. 01, 2017, *Springer Verlag*. doi: 10.1007/s13201-015-0367-y.

[2] B. Viswanathan, "Photocatalytic Degradation of Dyes: An Overview," *Current Catalysis*, vol. 7, no. 2, pp. 99–121, Dec. 2017, doi: 10.2174/2211544707666171219161846.

[3] A. Rafiq *et al.*, "Photocatalytic degradation of dyes using semiconductor photocatalysts to clean industrial water pollution," May 25, 2021, *Korean Society of Industrial Engineering Chemistry*. doi: 10.1016/j.jiec.2021.02.017.

[4] D. Gümüş and F. Akbal, "Photocatalytic degradation of textile dye and wastewater," *Water Air Soil Pollut*, vol. 216, no. 1–4, pp. 117–124, Mar. 2011, doi: 10.1007/s11270-010-0520-z.

[5] R. L. Singh, P. K. Singh, and R. P. Singh, "Enzymatic decolorization and degradation of azo dyes - A review," Oct. 01, 2015, *Elsevier Ltd*. doi: 10.1016/j.ibiod.2015.04.027.

[6] R. S. Sutar, R. P. Barkul, and M. K. Patil, "Sunlight assisted photocatalytic degradation of different organic pollutants and simultaneous degradation of cationic and anionic dyes using titanium and zinc based nanocomposites," *J Mol Liq*, vol. 340, Oct. 2021, doi: 10.1016/j.molliq.2021.117191.

[7] M. Soleimani, J. B. Ghasemi, G. Mohammadi Ziarani, H. Karimi-Maleh, and A. Badiei, "Photocatalytic degradation of organic pollutants, viral and bacterial pathogens using titania nanoparticles," Aug. 01, 2021, *Elsevier B.V.* doi: 10.1016/j.inoche.2021.108688.

[8] R. R. Elmorsi *et al.*, "Adsorption of Methylene Blue and Pb 2+ by using acid-activated Posidonia oceanica waste," *Sci Rep*, vol. 9, no. 1, Dec. 2019, doi: 10.1038/s41598-019-39945-1.

[9] M. Nasrollahzadeh, Z. Issaabadi, and S. M. Sajadi, "Green synthesis of a Cu/MgO nanocomposite by: Cassytha filiformis L. extract and investigation of its catalytic activity in the reduction of methylene blue, congo red and nitro compounds in aqueous media," *RSC Adv*, vol. 8, no. 7, pp. 3723–3735, 2018, doi: 10.1039/c7ra13491f.

[10] J. M. Poyatos, M. M. Muñio, M. C. Almecija, J. C. Torres, E. Hontoria, and F. Osorio, "Advanced oxidation processes for wastewater treatment: State of the art," *Water Air Soil Pollut*, vol. 205, no. 1–4, pp. 187–204, Jan. 2010, doi: 10.1007/s11270-009-0065-1.

[11] S. P. Onkani, P. N. Diagboya, F. M. Mtunzi, M. J. Klink, B. I. Olu-Owolabi, and V. Pakade, "Comparative study of the photocatalytic degradation of 2–chlorophenol under UV irradiation using pristine and Ag-doped species of TiO2, ZnO and ZnS photocatalysts," *J*

Environ Manage, vol. 260, Apr. 2020, doi: 10.1016/j.jenvman.2020.110145.

[12] A. Kumar *et al.*, "Recent advances in nano-Fenton catalytic degradation of emerging pharmaceutical contaminants," Sep. 15, 2019, *Elsevier B.V.* doi: 10.1016/j.molliq.2019.111177.

[13] H. Yin, Y. Zhou, C. Sui, J. Ding, and J. Wang, "Recent advances on photocatalytic degradation of phthalate ester plasticizers using nanomaterial photocatalysts," Jul. 01, 2025, *Academic Press Inc.* doi: 10.1016/j.envres.2025.121497.

[14] N. S. Davamani, J. Mariadhas, P. M. D. Samuel, and S. R. I. Savariroyan, "The effect of Mg doping on structural and catalytic removal of malachite green using ZnO thin films fabrication by cost effective home-made spray pyrolysis technique," *Next Materials*, vol. 8, Jul. 2025, doi: 10.1016/j.nxmate.2025.100884.

[15] D. P. Das and K. M. Parida, "Solar light induced photocatalytic degradation of pollutants over titania pillared zirconium phosphate and titanium phosphate," *Catalysis Surveys from Asia*, vol. 12, no. 3, pp. 203–213, Sep. 2008, doi: 10.1007/s10563-008-9052-6.

[16] S. Sarkar and K. K. Chattopadhyay, "Visible light photocatalysis and electron emission from porous hollow spherical BiVO4 nanostructures synthesized by a novel route," *Physica E Low Dimens Syst Nanostruct*, vol. 58, pp. 52–58, Apr. 2014, doi: 10.1016/j.physe.2013.11.014.

[17] S. Ahmed, M. G. Rasul, W. N. Martens, R. Brown, and M. A. Hashib, "Advances in heterogeneous photocatalytic degradation of phenols and dyes in wastewater: A review," *Water Air Soil Pollut*, vol. 215, no. 1–4, pp. 3–29, Feb. 2011, doi: 10.1007/s11270-010-0456-3.

[18] A. García *et al.*, "Detoxification of aqueous solutions of the pesticide 'Sevnol' by solar photocatalysis," *Environ Chem Lett*, vol. 3, no. 4, pp. 169–172, 2006, doi: 10.1007/s10311-005-0026-x.

[19] S. Tariq, A. Ahmed, S. Saad, and S. Tariq, "Structural, electronic and elastic properties of the cubic CaTiO3 under pressure: A DFT study," *AIP Adv*, vol. 5, no. 7, Jul. 2015, doi: 10.1063/1.4926437.

[20] J. Pan *et al.*, "The enhanced photocatalytic hydrogen production of the fusiform g-C3N4 modification CaTiO3 nano-heterojunction," *Int J Hydrogen Energy*, vol. 43, no. 41, pp. 19019–19028, Oct. 2018, doi: 10.1016/j.ijhydene.2018.08.102.

[21] L. Bai, Q. Xu, and Z. Cai, "Synthesis of Ag@AgBr/CaTiO3 composite photocatalyst with enhanced visible light photocatalytic activity," *Journal of Materials Science: Materials in Electronics*, vol. 29, no. 20, pp. 17580–17590, Oct. 2018, doi: 10.1007/s10854-018-9861-y.

[22] A. Bhava, U. S. Shenoy, and D. K. Bhat, "Silver doped barium titanate nanoparticles for

enhanced visible light photocatalytic degradation of dyes," *Environmental Pollution*, vol. 344, Mar. 2024, doi: 10.1016/j.envpol.2024.123430.

[23] M. F. Mehmood and A. Habib, "Hydrothermal Synthesis and Structural Characterization of BaTiO3 Powder," *The Nucleus*, vol. 60, no. 2, pp. 168–173, Sep. 2023, doi: 10.71330/thenucleus.2023.1296.

[24] R. Vijayalakshmi and V. Rajendran, "SYNTHESIS AND CHARACTERIZATION OF CUBIC BaTiO 3 NANORODS VIA FACILE HYDROTHERMAL METHOD AND THEIR OPTICAL PROPERTIES," 2010.

[25] M. Passi and B. Pal, "Influence of Ag/Cu photodeposition on CaTiO3 photocatalytic activity for degradation of Rhodamine B dye," *Korean Journal of Chemical Engineering*, vol. 39, no. 4, pp. 942–953, Apr. 2022, doi: 10.1007/s11814-021-0975-1.

[26] L. Bai, Q. Xu, and Z. Cai, "Synthesis of Ag@AgBr/CaTiO3 composite photocatalyst with enhanced visible light photocatalytic activity," *Journal of Materials Science: Materials in Electronics*, vol. 29, no. 20, pp. 17580–17590, Oct. 2018, doi: 10.1007/s10854-018-9861-y.

[27] M. S. Hamdy, H. S. M. Abd-Rabboh, M. Benaissa, M. G. Al-Metwaly, A. H. Galal, and M. A. Ahmed, "Fabrication of novel polyaniline/ZnO heterojunction for exceptional photocatalytic hydrogen production and degradation of fluorescein dye through direct Z-scheme mechanism," *Opt Mater (Amst)*, vol. 117, Jul. 2021, doi: 10.1016/j.optmat.2021.111198.

[28] D. Gogoi, A. Namdeo, A. K. Golder, and N. R. Peela, "Ag-doped TiO2 photocatalysts with effective charge transfer for highly efficient hydrogen production through water splitting," *Int J Hydrogen Energy*, vol. 45, no. 4, pp. 2729–2744, Jan. 2020, doi: 10.1016/j.ijhydene.2019.11.127.

[29] S. Krejčíková *et al.*, "Preparation and characterization of Ag-doped crystalline titania for photocatalysis applications," *Appl Catal B*, vol. 111–112, pp. 119–125, Jan. 2012, doi: 10.1016/j.apcatb.2011.09.024.

[30] A. Soni, S. Mishra, D. Vaya, and P. K. Surolia, "Role of Ag and g-C3N4 over CaTiO3 for effective photocatalytic degradation of nitrobenzene," *Inorg Chem Commun*, vol. 159, Jan. 2024, doi: 10.1016/j.inoche.2023.111862.

[31] M. de la Garza-Galván *et al.*, "In situ synthesis of Au-decorated BiOCl/BiVO4 hybrid ternary system with enhanced visible-light photocatalytic behavior," *Appl Surf Sci*, vol. 487, pp. 743–754, Sep. 2019, doi: 10.1016/j.apsusc.2019.05.041.

[32] X. Xue, X. Chen, and X. Gong, "Fast electron transfer and enhanced visible light photocatalytic activity of silver and Ag2O co-doped titanium dioxide with the doping of electron mediator for removing gaseous toluene," *Mater Sci Semicond Process*, vol. 132,

Sep. 2021, doi: 10.1016/j.mssp.2021.105901.

[33] X. Wang, X. Bai, Z. Pang, H. Yang, and Y. Qi, "Investigation of surface plasmons in Kretschmann structure loaded with a silver nano-cube," *Results Phys*, vol. 12, pp. 1866–1870, Mar. 2019, doi: 10.1016/j.rinp.2019.02.002.

[34] I. Khan *et al.*, "Review on Methylene Blue: Its Properties, Uses, Toxicity and Photodegradation," Jan. 01, 2022, *MDPI*. doi: 10.3390/w14020242.

[35] H. D. Bouras *et al.*, "Biosorption characteristics of methylene blue dye by two fungal biomasses," *International Journal of Environmental Studies*, vol. 78, no. 3, pp. 365–381, 2021, doi: 10.1080/00207233.2020.1745573.

[36] M. Passi and B. Pal, "Design of a novel Ag-BaTiO3/GO ternary nanocomposite with enhanced visible-light driven photocatalytic performance towards mitigation of carcinogenic organic pollutants," *Sep Purif Technol*, vol. 308, Mar. 2023, doi: 10.1016/j.seppur.2022.122839.

[37] T. Fafal, P. Taştan, B. S. Tüzün, M. Ozyazici, and B. Kivcak, "Synthesis, characterization and studies on antioxidant activity of silver nanoparticles using Asphodelus aestivus Brot. aerial part extract," *South African Journal of Botany*, vol. 112, pp. 346–353, Sep. 2017, doi: 10.1016/j.sajb.2017.06.019.

[38] S. Kappadan, S. Thomas, and N. Kalarikkal, "BaTiO3/ZnO heterostructured photocatalyst with improved efficiency in dye degradation," *Mater Chem Phys*, vol. 255, Nov. 2020, doi: 10.1016/j.matchemphys.2020.123583.

[39] Z. Wu *et al.*, "High piezo-photocatalysis of BaTiO3 nanofibers for organic dye decomposition," May 01, 2024, *Elsevier B.V.* doi: 10.1016/j.surfin.2024.104308.

[40] L. Chen, S. F. Ou, T. B. Nguyen, Y. Chuang, C. W. Chen, and C. Di Dong, "In-situ hydrothermal synthesis of MoS2 /TiO2 nanocomposites for enhanced and stable photocatalytic performance: Methylene blue degradation pathway and mechanism," *J Taiwan Inst Chem Eng*, vol. 166, Jan. 2025, doi: 10.1016/j.jtice.2024.105436.

[41] X. Yu *et al.*, "Ag-Cu2O composite films with enhanced photocatalytic activities for methylene blue degradation: Analysis of the mechanism and the degradation pathways," *J Environ Chem Eng*, vol. 9, no. 5, Oct. 2021, doi: 10.1016/j.jece.2021.106161.

Plag Report:


QuillBot
QuillBot
Scanned on: 05:29 July 31, 2025 UTC
11.5%
Overall similarity score
33
Results found
8491
Total words in text
Word count
Identical 369
Minor Changes 219
Paraphrased 392
Omitted 0
Powered by COPYLEAKS